Managing Shared Mobility Systems with Electric Vehicles Under Correlated Demand Uncertainties

(Authors' names blinded for peer review)

Problem definition: Using electric vehicles (EVs) with vehicle-to-grid (V2G) technology in a shared mobility system promotes sustainability but limits vehicle accessibility. This highlights the importance of optimizing the initial EV allocation, which should also consider subsequent operational decisions. The problem is further complicated by correlated uncertainties in trip demands across service regions and time periods without perfect knowledge of these correlations.

Methodology/results: We propose a two-stage distributionally robust optimization (DRO) model considering ambiguously correlated trip-demand uncertainties. In the first stage, an operator decides the initial vehicle allocation. In the second stage, the operator determines various operational decisions to meet demands over a time horizon. The objective is to minimize the expected cost under a worst-case joint distribution within an ambiguity set based on moment information of the correlated uncertainties. We show a monotonic relationship between the optimal objective value and the trip-demand covariance matrix. We further prioritize trip-demand pairs based on their covariance value or shadow price, enabling us to focus on a subset of demand pairs, which is especially appealing given the operator's limited resources. To improve computational efficiency, we propose tight approximations of the DRO model based on principal component analysis and develop a hybrid algorithm using a temporal decomposition technique. Numerical results based on real data confirm our approach's efficiency.

Managerial implications: It is crucial to properly incorporate correlation information, which can attain up to 4.66% total cost reduction. Furthermore, EVs mostly charge during the early hours when electricity prices and trip demands are low and discharge when prices are high. The peaks of relocation deviate from the peaks of charging of EVs. Faster charging reduces the EV allocation and total cost. We observe more frequent charging of EVs under a time-based pricing scheme for charging compared to an amount-based pricing scheme.

Key words: Shared Mobility; Electric Vehicles; Vehicle-to-grid; Distributionally Robust Optimization; Principal Component Analysis

1. Introduction

Shared mobility systems have gained popularity in many cities worldwide, with an annual growth rate of 30% (Soppert et al. 2022). They contribute to sustainability (Qi et al. 2018, Benjaafar and Hu 2020, Zhang et al. 2021) by offering a flexible way of transportation, while reducing traffic congestion and greenhouse gas (GHG) emissions. Recently, the rising popularity of electric vehicles (EVs) has further enhanced the shared mobility systems' contribution to sustainability as EVs can potentially save a significant amount of GHG emissions. According to Zipcar (2024), switching 120,000 private vehicles to 9,000 shared EVs could potentially reduce emissions by nearly 160,000 tons annually. Given their high potential, many car-sharing companies are transitioning

from a fleet of fossil-fuel vehicles to a fleet of EVs. For example, Uber aims to have 50% of trips covered by EVs in key European cities by 2025, and 100% by 2040 (Uber 2023), while Zipcar has allocated more than 600 EVs across London and aims to upgrade its fleet to fully electric by 2025 (Zipcar 2024). We call such shared mobility systems with EVs as *EV-shared mobility systems*.

The sustainability benefits of EV-shared mobility systems are further amplified by vehicle-to-grid (V2G) technology. With V2G technology, EVs can discharge their stored electricity to the power grid and serve as massive batteries collectively (Ai et al. 2021). This helps stabilize the power grid's electricity generation, thereby cutting its fuel wastes, GHG emissions, and pollution. Meanwhile, V2G technology also presents opportunities to generate revenues for EV-shared mobility systems by discharging electricity to the power grid. As a result, V2G technology has been warmly embraced by EV owners, power systems, and governments worldwide. For example, State Grid in China collaborated with Great Wall Motor Group to initiate a large V2G project in Baoding, China, in 2021 (Grasen 2021). Pacific Gas and Electric Company in the U.S. obtained government approval to launch the nation's first V2G compensation program for commercial EV owners in California in 2022 (Nasdaq 2022). E.ON, an energy network operator in the U.K., partnered with Nissan to install 20 V2G points in Cranfield, U.K. in 2020 (Zapmap 2020).

Using EVs with V2G technology in a shared mobility system presents substantial challenges for determining the initial vehicle allocation (i.e., the number of EVs allocated). In particular, EVs can only charge or discharge at certain locations with specific facilities. The charging and discharging processes are time-consuming, rendering EVs unavailable for serving trip demands during a certain duration. This implies that introducing EVs with V2G technology may affect EV accessibility, and adjusting EV allocation can offset this effect. Unfortunately, dynamically adjusting the number of EVs over time is prohibitively expensive given the high cost of owning the EVs. This highlights the importance of optimizing the initial vehicle allocation at the start of a time horizon for an EV-shared mobility system with V2G technology. Since the initial EV allocation significantly influences subsequent system operations, it is crucial to take various EV operations (including demand fulfillment, relocation, charging, and discharging) into account when optimizing allocation decisions. This motivates an integrated model for jointly optimizing both allocation and operational decisions over the time horizon.

The above problem is especially challenging because of the uncertain nature of trip demands, which arises from various causes, including traffic congestion and weather conditions (Zhang and Kincaid 2014). To ensure effective EV allocation and operations, one needs to take the trip-demand uncertainty into consideration. Furthermore, the uncertain trip demands across different service regions and time periods are often correlated. For example, Figure 1 presents the correlations of trip demands at 6:00, 12:00, and 18:00 in Manhattan, New York City (NYC). Apparently, the trip

demands at these times can be highly correlated. Specifically, demands at 6:00 have a stronger correlation with demands at 18:00 than with those at 12:00. Additionally, the correlation between trip demands at 12:00 and 18:00 is stronger than the correlation between trip demands at 6:00 and 18:00. Furthermore, we also examine correlations across different service regions. Specifically, we analyze daily trip demands in three types of regions: office, residence, and commerce[1]. Figure 2 suggests that trip demands in different regions can also exhibit strong correlations. For example, trip demands in the office region are more strongly correlated with those in the commerce region than with the residence region, while trip demands in the residence region are more strongly correlated with those in the office region than with the commerce region.

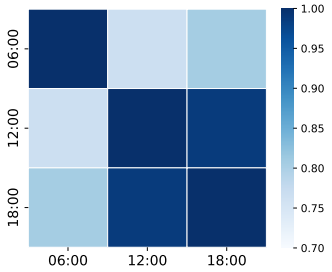

Figure 1 **Temporal Correlation**

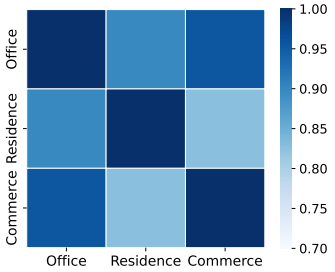

Figure 2 **Spatial Correlation**

Our numerical experiments in Section 7.3 will demonstrate that it is important to take the trip-demand correlations into consideration because this can lead to significantly better performance. For example, when trip demands in two different periods are positively correlated, we can anticipate a future rise in demand based on an earlier increase. Thus, we can relocate EVs in advance once we observe an early demand increase to ensure sufficient EV availability for later periods. To consider correlations of trip-demand pairs across *all* service regions and time periods, it requires a high-dimensional matrix. However, given the limited resources of the operator, obtaining such a matrix is almost impossible in practice. Thus, it is necessary for the operator to consider uncertain and correlated trip demands without perfect knowledge of the correlations.

In this paper, we focus on *initial allocation* and *subsequent operations* of an EV-shared mobility system with V2G technology under *correlated trip-demand uncertainty*. In particular, we would like to answer the following research questions: (i) How should we formulate a model for an operator of the EV-shared mobility system to strategically match its finite EV supply with uncertain and correlated trip demands by optimizing its EV allocation and operations such that its cost is minimized? (ii) Can we find a computationally tractable approach to solving such a model on a practical scale? How does incorporating different information of demand correlations affect our solution approach's performance? Given limited resources, how should the operator prioritize trip-demand pairs without perfect knowledge of their correlations? (iii) Are there any interesting features in EV charging and discharging during the operations? How do various parameters

impact the system's performance? Besides charging and discharging, are there any other EV operations that have interesting features?

To answer these questions, we consider an operator with a fleet of EVs serving uncertain and correlated trip demands across service regions over an operational horizon with multiple periods. We assume that the electricity charging and discharging prices may fluctuate over time. At the start of the horizon, the operator decides the initial EV allocation for each region without knowing the trip demands. After the demands in each period are realized, the operator determines (and executes) demand fulfillment, relocation, charging, and discharging decisions. We formulate the problem using a two-stage model. To take correlated trip-demand uncertainty into consideration without its full information, we adopt a moment-based distributionally robust optimization (DRO) approach. This modeling framework integrates statistical information of uncertain parameters with an optimization method (Scarf 1958, Goh and Sim 2010). There are several advantages of using DRO to optimize EV allocation and operations under correlated demand uncertainty: (i) DRO does not need perfect knowledge of the correlations. (ii) DRO optimizes the decisions under a worst-case distribution, which are robust against correlation variability. (iii) Increasing the data amount can enrich the statistical information, thereby enhancing DRO's solution quality without adversely affecting the problem size. This is particularly relevant and important for the evolving EV-shared mobility systems, where the amount of data is growing quickly.

We summarize our main results and contributions as follows.

(i) **Developing a new modeling approach for the problem:** We construct a two-stage DRO model to optimize vehicle allocation and operations for an EV-shared mobility system with V2G technology under correlated trip-demand uncertainty. In the first stage, the operator decides the EV allocation for each service region. In the second stage, the operator determines the EV operational decisions (including charging and discharging) over the horizon. Using limited data, the proposed DRO model incorporates trip-demand correlations in an ambiguity set based on the support as well as the first- and second-moment information of demand uncertainty. To make the two-stage DRO model tractable, we reformulate it as a semidefinite programming (SDP) model.

(ii) **Reducing information requirement:** We show a monotonic relationship between the DRO model's optimal objective value and the covariance matrix of trip demands. We then identify upper and lower bounds on the optimal objective value, with the former considering all possible correlations and the latter assuming no correlations. To develop a practical approach with a good balance between these two extreme cases, we need to estimate the covariance of trip demands. We prioritize the trip-demand pairs based on their in-sample covariance value or shadow price, enabling us to focus on a subset of demand pairs. This is especially appealing given the operator's limited resources in practice to estimate the out-of-sample covariance for all demand pairs.

(iii) **Improving computational efficiency:** To improve the computational efficiency of solving the DRO model, we develop three approximation approaches, including outer and inner approximations using principal component analysis (PCA) and an approximation that considers a subset of feasible solutions. Finally, we propose a hybrid algorithm that integrates a temporal decomposition technique with the above three approaches to further speed up the computation.
(iv) **Providing managerial insights:** Our study yields the following managerial insights for EV-shared mobility systems with V2G technology. Most EVs are relocated from regions with an oversupply to regions with shortages when trip demands significantly rise. Most EVs finish charging during the early hours when the charging price and the total trip demand are low, and some EVs charge before the price increases and after the price drops. The peaks of relocation deviate from the peaks of charging of EVs. Furthermore, a larger charging speed reduces the EV allocation and total cost. A time-based pricing scheme for charging EVs leads to more charging peaks and a larger total discharging amount compared to an amount-based pricing scheme.

After reviewing the related literature in Section 2, we present a two-stage stochastic model in Section 3. Section 4 introduces the DRO model and its tractable reformulation. Section 5 investigates the impact of incorporating different information of demand correlations. Section 6 proposes the approximation approaches and hybrid algorithm. Section 7 conducts numerical experiments to assess the algorithm. Section 8 concludes the paper. All proofs can be found in the appendix.

2. Related Literature

The field of shared mobility has drawn notable attention because of its value in urban transportation and sustainability. In a shared mobility system, a customer can rent a vehicle for a short trip (e.g., Nair and Miller-Hooks 2011 and Benjaafar et al. 2022). Many papers on shared mobility focus on bikes and fossil-fuel vehicles (Jin et al. 2023). Shu et al. (2013) develop two linear programming models to optimize bike allocation and operations in a bike-shared mobility system. Liu et al. (2016) optimize bike rebalancing decisions by solving a large-scale routing problem in a bike-shared mobility system. Lu et al. (2018) propose a two-stage stochastic model to optimize fossil-fuel vehicle allocation and operations under uncertain trip demands. He et al. (2021b) take bike stations' geographic locations into account and provide guidance for a network design in a bike-shared mobility system. Chen et al. (2024) optimize dynamic pricing and relocation decisions to balance vehicle supply and trip demands in a ride-hailing system.

Different from shared bikes or fossil-fuel vehicles, shared EVs face additional challenges in optimizing charging and discharging during operations. Our work is closely related to the Operations Management (OM)/Operations Research (OR) literature on EV-shared mobility systems. He et al. (2017) study a service region design problem in an EV-shared mobility system to maximize trip

demand satisfaction while controlling the operation cost. He et al. (2021a) develop an integrated queuing-location model to jointly optimize charging facilities planning and EV charging operations in an EV-shared mobility system. Dong et al. (2022) develop a Markov decision process model to dynamically manage EVs with a low battery level for charging and EVs with a high battery level for serving customers, aiming to minimize customer waiting time and demand loss.

Recently, some studies have further extended the work in planning and operations of an EV-shared mobility system by incorporating V2G technology, which are more closely aligned with our paper. Widrick et al. (2018) employ a Markov decision process model to optimize EV battery swaps at exchange stations, accounting for uncertain demands in an EV-shared mobility system with V2G technology. Qi et al. (2022) explore an EV-shared mobility system connected with an urban microgrid through V2G technology. They formulate deterministic models to optimize EV fleet dispatch and electricity exchange. Lauinger et al. (2024) design a nonconvex robust optimization model to effectively manage the sale of primary frequency regulation through V2G technology, aiming to maximize expected profits for the vehicle owner facing uncertain demands. Zhang et al. (2021) develop a two-stage stochastic model to optimize EV allocation and operations based on the assumption that trip-demand correlations are perfectly known. However, estimating the exact trip-demand correlations in practice is challenging, if not impossible. We contribute to this stream of literature by optimizing the allocation and operations of EVs, considering the correlations of trip-demand pairs across all service regions and time periods, without requiring perfect knowledge of these correlations. This enables us to obtain more reliable solutions for the allocation and operations of EVs even when data is limited.

Our methodology is based on DRO, which identifies an optimal solution under a worst-case distribution. Unlike stochastic optimization (SO), DRO does not require perfect knowledge of trip-demand uncertainties, enhancing the solution's practical applicability, especially in situations with limited data. In contrast to robust optimization (RO), DRO incorporates additional information on trip-demand uncertainties, making the solution less conservative. As a result, DRO has received substantial attention. Delage and Ye (2010) propose a moment-based DRO model with an ambiguity set considering the mean and covariance of uncertainties. They further reformulate the model as a semidefinite program (SDP), which can be solved in polynomial time. Wiesemann et al. (2014) propose a unifying framework for modeling and solving a DRO problem with an ambiguity set containing all distributions with mean values residing on an affine manifold and with conic representable confidence sets. Esfahani and Kuhn (2017) propose a DRO model with the Wasserstein metric and its tractable reformulation. Gao (2023) investigate finite-sample guarantees for a DRO model with the Wasserstein metric. In addition to provable performance

guarantees, DRO also demonstrates practical success across a wide range of applications, including inventory management (Xin and Goldberg 2022, Cui et al. 2023), transportation or networks (Ghosal and Wiesemann 2020, He et al. 2020, Basciftci et al. 2021, Li et al. 2024), and power systems (Alismail et al. 2017, Fathabad et al. 2020). For a comprehensive discussion of DRO, we refer interested readers to Rahimian and Mehrotra (2019).

3. Problem Formulation

Consider a shared electrical vehicle (EV) firm that operates an EV fleet, where each EV's state-of-charge (SoC) is $s \in \mathcal{S} = \{1, 2, \ldots, S\}$. The firm, also known as the operator, provides shared mobility service for each region $z \in \mathcal{Z} = \{1, 2, \ldots, Z\}$ in each period $t \in \mathcal{T} = \{0, 1, \ldots, T\}$. For example, a service region is a sub-area of Manhattan in New York City, and a period corresponds to a 10-minute interval. To capture the movement of EVs with various SoCs across service regions in different periods, we first establish a *time-space-SoC network* in Section 3.1. Based on this network, we construct a two-stage optimization model in Sections 3.2 and 3.3.

3.1. Time-space-SoC Network

We model the movement of EVs with various SoCs across regions and periods as *flows* in a time-space-SoC network $\mathcal{G} = (\mathcal{N}, \mathcal{A})$, where $\mathcal{N}$ is a set of nodes and $\mathcal{A}$ is a set of directed arcs in the network as shown in Figure 3. Let $n_{z,t,s}$ denote a node in $\mathcal{N}$ that corresponds to region z in period t with SoC state s, for $z \in \mathcal{Z}$, $t \in \mathcal{T}$, $s \in \mathcal{S}$. Let $(n_{z,t,s}, n_{z',t',s'})$ denote a directed arc in $\mathcal{A}$ that connects node $n_{z,t,s}$ to node $n_{z',t',s'}$ in the network $\mathcal{G}$.

Based on how EVs are transferred between any two nodes in the network $\mathcal{G}$, we define five types of arcs in $\mathcal{A}$:

(i) *Rental arcs*: This set of arcs, denoted by $\mathcal{A}^{\mathrm{R}}$, corresponds to rental trips of EVs. Specifically, the flow on each rental arc $(n_{z,t,s}, n_{z',t',s'}) \in \mathcal{A}^{\mathrm{R}}$ represents the number of EVs for rental trips starting from region z in period t with SoC s and ending at region $z' \neq z$ in period $t' = t + \ell_{z,z'}$ with SoC $s' = s - b_{z,z'}$, where $\ell_{z,z'}$ and $b_{z,z'}$ denote the number of periods and the number of SoC units an EV requires to move from region z to region z'. Define $\mathcal{W}^{\mathrm{R}} := \{(z, z', t, t', s, s') \in \mathcal{Z} \times \mathcal{Z} \times \mathcal{T} \times \mathcal{T} \times \mathcal{S} \times \mathcal{S} \mid (n_{z,t,s}, n_{z',t',s'}) \in \mathcal{A}^{\mathrm{R}}\}$.

(ii) *Idle arcs*: This set of arcs, denoted by $\mathcal{A}^{\mathrm{I}}$, corresponds to idle EVs. In particular, the flow on each idle arc $(n_{z,t,s}, n_{z,t+1,s}) \in \mathcal{A}^{\mathrm{I}}$ represents the number of EVs in region z with SoC s that are idle from period t to period $t+1$. Define $\mathcal{W}^{\mathrm{I}} := \{(z, t, s) \in \mathcal{Z} \times \mathcal{T} \times \mathcal{S} \mid (n_{z,t,s}, n_{z,t+1,s}) \in \mathcal{A}^{\mathrm{I}}\}$.

(iii) *Relocation arcs*: This set of arcs, denoted by $\mathcal{A}^{\mathrm{L}}$, corresponds to EV relocation. Specifically, the flow on each relocation arc $(n_{z,t,s}, n_{z',t',s}) \in \mathcal{A}^{\mathrm{L}}$ represents the number of EVs relocated from region z in period t with SoC s to region $z' \neq z$ in period $t' = t + \ell_{z,z'}$. Define $\mathcal{W}^{\mathrm{L}} := \{(z, z', t, t', s) \in \mathcal{Z} \times \mathcal{Z} \times \mathcal{T} \times \mathcal{T} \times \mathcal{S} \mid (n_{z,t,s}, n_{z',t',s}) \in \mathcal{A}^{\mathrm{L}}\}$.

(iv) *Charging arcs*: This set of arcs, denoted by $\mathcal{A}^{\mathrm{C}}$, corresponds to charging of EVs. In particular, the flow on each charging arc $(n_{z,t,s}, n_{z,t+1,s'}) \in \mathcal{A}^{\mathrm{C}}$ represents the number of EVs in region z and period t with SoC s that are charged to $s' = \min\{s + \delta^{\mathrm{C}}, S\}$ after 1 period, where δ^{C} denotes the charging amount per period (charging rate). Define $\mathcal{W}^{\mathrm{C}} := \{(z,t,s,s') \in \mathcal{Z} \times \mathcal{T} \times \mathcal{S} \times \mathcal{S} \mid (n_{z,t,s}, n_{z,t+1,s'}) \in \mathcal{A}^{\mathrm{C}}\}$.

(v) *Discharging arcs*: This set of arcs, denoted by $\mathcal{A}^{\mathrm{E}}$, corresponds to discharging of EVs. Specifically, the flow on each discharging arc $(n_{z,t,s}, n_{z,t+1,s'}) \in \mathcal{A}^{\mathrm{E}}$ represents the number of EVs in region z and period t with SoC s that are discharged to $s' = \max\{s - \delta^{\mathrm{E}}, 0\}$ after 1 period, where δ^{E} denotes the discharging amount per period (discharging rate). Define $\mathcal{W}^{\mathrm{E}} := \{(z,t,s,s') \in \mathcal{Z} \times \mathcal{T} \times \mathcal{S} \times \mathcal{S} \mid (n_{z,t,s}, n_{z,t+1,s'}) \in \mathcal{A}^{\mathrm{E}}\}$.

Figure 3 gives an example of each of the five types of arcs, which constitute all the arcs of the network $\mathcal{G}$. That is, $\mathcal{A} = \mathcal{A}^{\mathrm{R}} \cup \mathcal{A}^{\mathrm{I}} \cup \mathcal{A}^{\mathrm{L}} \cup \mathcal{A}^{\mathrm{C}} \cup \mathcal{A}^{\mathrm{E}}$. Based on the network $\mathcal{G} = (\mathcal{N}, \mathcal{A})$, we formulate the firm's *integrated EV allocation and operations problem* as a two-stage optimization model. In the first stage, the firm decides the initial number of EVs with a certain SoC allocated to each service region, whereas in the second stage, the EV operational decisions (including rental, idle, relocation, charging, and discharging decisions) are made for the entire operational horizon.

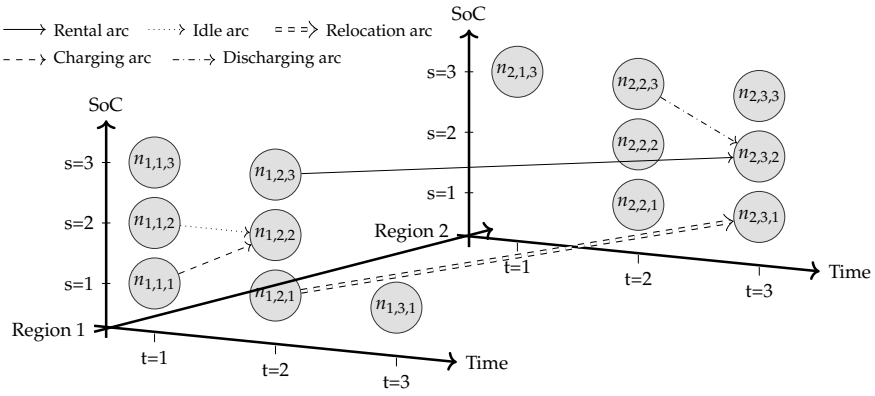

Figure 3 Time-space-SoC Network

3.2. First-stage Formulation

Let $x_{z,s}$ denote the number of EVs with SoC s allocated to region z, for $z \in \mathcal{Z}$, $s \in \mathcal{S}$. In the first stage, the operator makes the allocation decisions $x_{z,s}$ without knowing the demands. The operator is endowed with a budget that can afford at most $\overline{X}$ EVs such that

$$\sum_{z \in \mathcal{Z}} \sum_{s \in \mathcal{S}} x_{z,s} \leq \overline{X}. \tag{1}$$

Typically, the number of parked vehicles in a region is regulated by the government by controlling the number of parking spots. These parking spots are categorized into three types: spots without charging or discharging facilities (called type I), spots with charging facilities (called type

C), and spots with bi-directional charging facilities (called type E). Let $\mathcal{K} = \{\mathrm{I}, \mathrm{C}, \mathrm{E}\}$ denote the set of parking-spot types. Define X_z^k as the number of parking spots of type k in region z, for $k \in \mathcal{K}$, $z \in \mathcal{Z}$. Due to the regulations on the number of parked vehicles, we have

$$\sum_{s\in\mathcal{S}} x_{z,s} \leq \sum_{k\in\mathcal{K}} X_z^k, \ \forall z \in \mathcal{Z}. \tag{2}$$

A cost $c_s(\geq 0)$ is incurred for allocating an EV with SoC s to any region. Facing uncertain demands that follow a distribution $\mathbb{P}$, the operator makes its initial *allocation decisions in the first stage* and subsequent *operational decisions in the second stage* to minimize its expected total cost under the distribution $\mathbb{P}$. Let $\boldsymbol{\xi}$ denote a vector of (demand) uncertainties and let $\hat{\boldsymbol{\xi}}$ denote its realization. Given the first-stage decisions $\mathbf{x} = (x_{z,s}, z \in \mathcal{Z}, s \in \mathcal{S})^\top$ and a realization vector $\hat{\boldsymbol{\xi}}$ of uncertainties, we let $f(\mathbf{x}, \hat{\boldsymbol{\xi}})$ denote the optimal operations cost in the second stage. The operator optimizes its allocation decisions in the first stage by solving the following problem:

$$\min_{\mathbf{x}} \left\{ \sum_{z\in\mathcal{Z}} \sum_{s\in\mathcal{S}} c_s x_{z,s} + \mathbb{E}_{\mathbb{P}}\left[f\left(\mathbf{x}, \boldsymbol{\xi}\right)\right] \,\middle|\, (1)-(2) \right\}. \tag{$\mathcal{P}_1$}$$

3.3. Second-stage Formulation

We assume that at the beginning of the second stage, the uncertainties are realized as $\hat{\boldsymbol{\xi}}$. Thus, the operator knows the trip demand $d_{z,t,z'}(\hat{\boldsymbol{\xi}})$ starting from region z in period t and ending at region z' $(\neq z)$, for $z, z' \in \mathcal{Z}$, $t \in \mathcal{T}$. Define $\mathcal{M} := \{(z,t,z') \in \mathcal{Z} \times \mathcal{T} \times \mathcal{Z} \mid (n_{z,t,s}, n_{z',t',s'}) \in \mathcal{A}^{\mathrm{R}}\}$ as a set of indices of the starting regions, starting periods, and ending regions of all trip demands. Define a continuous decision variable $w_a(\hat{\boldsymbol{\xi}})$ as the flow (the number of vehicles) on arc a given the realization vector $\hat{\boldsymbol{\xi}}$, for $a \in \mathcal{A}$.

Let $\mathcal{A}_+(n_{z,t,s})$ and $\mathcal{A}_-(n_{z,t,s})$ denote the sets of arcs that originate from and terminate at $n_{z,t,s}$, respectively, for $n_{z,t,s} \in \mathcal{N}$. The number of EVs entering node $n_{z,t,s}$ should be the same as the number of EVs leaving this node, for $n_{z,t,s} \in \mathcal{N}$. Therefore, given the allocation decisions $\mathbf{x}$ in the first stage and the realization vector $\hat{\boldsymbol{\xi}}$, we have

$$\sum_{a\in\mathcal{A}_+(n_{z,0,s})} w_a(\hat{\boldsymbol{\xi}}) = x_{z,s}, \ \forall z \in \mathcal{Z}, s \in \mathcal{S}; \tag{3}$$

$$\sum_{a\in\mathcal{A}_+(n_{z,t,s})} w_a(\hat{\boldsymbol{\xi}}) = \sum_{a\in\mathcal{A}_-(n_{z,t,s})} w_a(\hat{\boldsymbol{\xi}}), \ \forall t \in \{1,\ldots,T-1\}, z \in \mathcal{Z}, s \in \mathcal{S}; \tag{4}$$

$$\sum_{z\in\mathcal{Z}} \sum_{s\in\mathcal{S}} \sum_{a\in\mathcal{A}_-(n_{z,T,s})} w_a(\hat{\boldsymbol{\xi}}) = \sum_{z\in\mathcal{Z}} \sum_{s\in\mathcal{S}} x_{z,s}. \tag{5}$$

Constraints (3) require that in period 0, the number of EVs leaving node $n_{z,0,s}$ equals the number of EVs with SoC s initially allocated to region z, for $z \in \mathcal{Z}, s \in \mathcal{S}$. Constraint (5) requires that the total number of EVs in all regions with any SoC in period T equals the total number of EVs allocated initially. Note that each trip demand can be served by EVs with various SoCs. That is, trip demand

$d_{z,t,z'}(\hat{\boldsymbol{\xi}})$, for $(z,t,z') \in \mathcal{M}$, can be served by EVs on any rental arc $(n_{z,t,s}, n_{z',t+\ell_{z,z'},s'}) \in \mathcal{A}^{\mathrm{R}}$. Thus, for $(z,t,z') \in \mathcal{M}$, we define a set $\hat{\mathcal{A}}^{\mathrm{R}}(z,t,z') := \{(n_{z,t,s}, n_{z',t+\ell_{z,z'},s'}) \in \mathcal{A}^{\mathrm{R}}\}$ to include all rental arcs that can serve trip demand $d_{z,t,z'}(\hat{\boldsymbol{\xi}})$. The total flow on all the arcs in $\hat{\mathcal{A}}^{\mathrm{R}}(z,t,z')$ should not exceed the demand $d_{z,t,z'}(\hat{\boldsymbol{\xi}})$. That is,

$$\sum_{a \in \hat{\mathcal{A}}^{\mathrm{R}}(z,t,z')} w_a(\hat{\boldsymbol{\xi}}) \leq d_{z,t,z'}(\hat{\boldsymbol{\xi}}),\ \forall\, (z,t,z') \in \mathcal{M}. \tag{6}$$

We now introduce the constraints related to the parking spots. For each type $k \in \mathcal{K}$ of parking spots, let $\mathcal{A}^k_+(n_{z,t,s})$ denote the set of arcs in $\mathcal{A}^k$ that originate from $n_{z,t,s}$, for $n_{z,t,s} \in \mathcal{N}$. Recall that X^k_z represents the number of parking spots of type k in region z. Specifically, we have

$$\sum_{s \in \mathcal{S}} \sum_{a \in \cup_{k \in \mathcal{K}} \mathcal{A}^k_+(n_{z,t,s})} w_a(\hat{\boldsymbol{\xi}}) \leq \sum_{k \in \mathcal{K}} X^k_z, \qquad \forall\, z \in \mathcal{Z},\, t \in \mathcal{T}; \tag{7}$$

$$\sum_{s \in \mathcal{S}} \sum_{a \in \mathcal{A}^{\mathrm{C}}_+(n_{z,t,s}) \cup \mathcal{A}^{\mathrm{E}}_+(n_{z,t,s})} w_a(\hat{\boldsymbol{\xi}}) \leq \sum_{k \in \{\mathrm{C},\mathrm{E}\}} X^k_z,\ \forall\, z \in \mathcal{Z},\, t \in \mathcal{T}; \tag{8}$$

$$\sum_{s \in \mathcal{S}} \sum_{a \in \mathcal{A}^{\mathrm{E}}_+(n_{z,t,s})} w_a(\hat{\boldsymbol{\xi}}) \leq X^{\mathrm{E}}_z, \qquad \forall\, z \in \mathcal{Z},\, t \in \mathcal{T}; \tag{9}$$

$$w_a(\hat{\boldsymbol{\xi}}) \geq 0, \qquad \forall\, a \in \mathcal{A}. \tag{10}$$

Constraints (7)–(9) require that the number of idle, charging, and discharging EVs in each region and period does not exceed the number of parking spots of the respective type. Constraints (10) ensure that the flow on each arc is non-negative.

Let $\mathbf{w}(\hat{\boldsymbol{\xi}}) = (w_a(\hat{\boldsymbol{\xi}}), a \in \mathcal{A})^\top$ denote a flow vector. Given the realization vector $\hat{\boldsymbol{\xi}}$, the operator optimizes its operational decisions in the second stage by solving the following problem:

$$f\left(\mathbf{x}, \hat{\boldsymbol{\xi}}\right) = \min_{\mathbf{w}(\hat{\boldsymbol{\xi}})} \left\{ \sum_{a \in \mathcal{A}} c_a w_a(\hat{\boldsymbol{\xi}}) + c_{\mathrm{P}} \sum_{(z,t,z') \in \mathcal{M}} \left(d_{z,t,z'}(\hat{\boldsymbol{\xi}}) - \sum_{a \in \hat{\mathcal{A}}^{\mathrm{R}}(z,t,z')} w_a(\hat{\boldsymbol{\xi}}) \right) \,\middle|\, (3)-(10) \right\}, \tag{$\mathcal{P}_2$}$$

where c_a denotes the unit cost of the flow on arc $a \in \mathcal{A}$ and c_{P} denotes the unit penalty cost for unsatisfied trip demands. Specifically, c_a can be determined as follows. (i) For rental arc $a = (n_{z,t,s}, n_{z',t',s'}) \in \mathcal{A}^{\mathrm{R}}$, we set $c_a = -c_{\mathrm{R}} \times \ell_{z,z'}$, where c_{R} is the rental per period. (ii) For idle arc $a = (n_{z,t,s}, n_{z,t+1,s}) \in \mathcal{A}^{\mathrm{I}}$, we set $c_a = c_{\mathrm{I}}$, where c_{I} is the idle cost per period. (iii) For relocation arc $a = (n_{z,t,s}, n_{z',t',s}) \in \mathcal{A}^{\mathrm{L}}$, we set $c_a = c_{\mathrm{L}} \times \ell_{z,z'}$, where c_{L} is the relocation cost per period. (iv) For charging arc $a = (n_{z,t,s}, n_{z,t+1,s'}) \in \mathcal{A}^{\mathrm{C}}$, we set $c_a = \beta^{\mathrm{C}}_{t,s,s'} := P^{\mathrm{C}}_t \times (s' - s) + c_{\mathrm{deg}}$, where P^{C}_t is the unit electricity charging price in period t and c_{deg} is the battery degradation cost. (v) For discharging arc $a = (n_{z,t,s}, n_{z,t+1,s'}) \in \mathcal{A}^{\mathrm{E}}$, we set $c_a = \beta^{\mathrm{E}}_{t,s,s'} = -P^{\mathrm{E}}_t \times (s - s') + c_{\mathrm{deg}}$, where P^{E}_t is the unit electricity discharging price in period t.

4. Distributionally Robust Optimization Model

As discussed in Section 1, the uncertain trip demands across all service regions and all periods are correlated. As a result, we have to take into account a comprehensive correlation matrix of all trip demands $d_{z,t,z'}(\boldsymbol{\xi}), (z,t,z') \in \mathcal{M}$, which could be very large. For example, even if we partition a geographical area into $Z = 5$ service regions and consider a day with $T = 144$ periods, the trip demand vector $\mathbf{d}(\boldsymbol{\xi}) = \{d_{z,t,z'}(\boldsymbol{\xi}), (z,t,z') \in \mathcal{M}\}$ has a dimension of $3,600$, and its covariance matrix has a dimension of $3,600 \times 3,600$. Consequently, to estimate the joint distribution of $\mathbf{d}(\boldsymbol{\xi})$, a significant amount of historical data is necessary. Unfortunately, such data is usually difficult to acquire in practice, if not impossible, given that EV sharing is a relatively new industry. To address these challenges, we employ moment-based DRO to deal with Problem ($\mathcal{P}_1$). DRO is a modeling framework that integrates statistical information (e.g., support, mean, and covariance) about uncertain parameters with an optimization method (Jiang et al. 2023). Under this framework, one can relax the assumption on the perfect knowledge of the true distribution $\mathbb{P}$ in Problem ($\mathcal{P}_1$). Instead, we only assume that $\mathbb{P}$ falls in a distributional ambiguity set constructed based on the statistical information and then optimize decisions against the worst-case distribution within this ambiguity set. We describe how to apply the DRO framework to Problem ($\mathcal{P}_1$) in detail below.

In moment-based DRO, we consider an ambiguity set that includes all distributions with support, mean, and covariance satisfying some prescribed conditions (Rahimian and Mehrotra 2019). Since the uncertain parameters in Problem ($\mathcal{P}_1$) are trip demands, we can use the vector of uncertainties $\boldsymbol{\xi}$ to represent the trip demand vector $\mathbf{d}(\boldsymbol{\xi}) = (d_{z,t,z'}, (z,t,z') \in \mathcal{M})^\top$ for the rest of the paper. Given the support set Ω, mean vector $\boldsymbol{\mu}$, and covariance matrix $\boldsymbol{\Sigma}$ of the vector of uncertainties $\boldsymbol{\xi}$, we define a moment-based ambiguity set below:

$$\mathcal{D}(\Omega, \boldsymbol{\mu}, \boldsymbol{\Sigma}, \gamma_1, \gamma_2) = \left\{ \mathbb{P} \middle| \begin{array}{l} \mathbb{P}(\boldsymbol{\xi} \in \Omega) = 1 \\ (\mathbb{E}_{\mathbb{P}}[\boldsymbol{\xi}] - \boldsymbol{\mu})^\top \boldsymbol{\Sigma}^{-1} (\mathbb{E}_{\mathbb{P}}[\boldsymbol{\xi}] - \boldsymbol{\mu}) \leq \gamma_1 \\ \mathbb{E}_{\mathbb{P}}\left[(\boldsymbol{\xi} - \boldsymbol{\mu})(\boldsymbol{\xi} - \boldsymbol{\mu})^\top\right] \preceq \gamma_2 \boldsymbol{\Sigma} \end{array} \right\}, \tag{11}$$

where parameters $\gamma_1 \geq 0$ and $\gamma_2 \geq 1$ are obtained from historical data. These parameters are used to control the size of the ambiguity set, which determines the conservatism of optimal solutions. The three constraints in $\mathcal{D}$ require that (i) any $\boldsymbol{\xi}$ lies in support set Ω; (ii) the mean of $\boldsymbol{\xi}$ lies in an ellipsoid of size γ_1 centered at $\boldsymbol{\mu}$; and (iii) the second-moment matrix is bounded by $\gamma_2 \boldsymbol{\Sigma}$ in a positive semi-definite (PSD) sense (Vazirani 2001), which helps capture *correlation information* explicitly. We assume $\Omega = \{\boldsymbol{\xi} \in \mathbb{R}^{|\mathcal{M}|} \mid \mathbf{b}^{\text{lb}} \leq \mathbf{A}\boldsymbol{\xi} \leq \mathbf{b}^{\text{ub}}\}$ is a polyhedron with at least one interior point. Here, $\mathbf{A}$ is an identity matrix with dimension $|\mathcal{M}| \times |\mathcal{M}|$, and $\mathbf{b}^{\text{lb}}, \mathbf{b}^{\text{ub}} \in \mathbb{R}^{|\mathcal{M}|}$ represent vectors of lower bounds and upper bounds of trip demands, respectively.

Instead of solving Problem ($\mathcal{P}_1$) with a given distribution, we minimize the expected cost under the worst-case distribution within a given ambiguity set $\mathcal{D}$ of probability distributions. That is,

$$\Gamma = \min_{\mathbf{x}} \left\{ \sum_{z\in\mathcal{Z}} \sum_{s\in\mathcal{S}} c_s x_{z,s} + \max_{\mathbb{P}\in\mathcal{D}} \mathbb{E}_{\mathbb{P}} \left[f\left(\mathbf{x}, \boldsymbol{\xi}\right) \right] \;\middle|\; (1)-(2) \right\}. \tag{$\mathcal{P}_{\mathrm{M}}$}$$

Note that Problem ($\mathcal{P}_{\mathrm{M}}$) has an inner max-min problem: $\max_{\mathbb{P}\in\mathcal{D}} \mathbb{E}_{\mathbb{P}}[f(\mathbf{x},\boldsymbol{\xi})]$. As such, Problem ($\mathcal{P}_{\mathrm{M}}$) is intractable its current form. Therefore, we will derive an equivalent reformulation of Problem ($\mathcal{P}_{\mathrm{M}}$) that is solvable. To achieve that, we first introduce an equivalent reformulation of the inner max-min problem of ($\mathcal{P}_{\mathrm{M}}$) in Theorem 1.

THEOREM 1. *The inner max-min problem:* $\max_{\mathbb{P}\in\mathcal{D}} \mathbb{E}_{\mathbb{P}}[f(\mathbf{x},\boldsymbol{\xi})]$ *of* ($\mathcal{P}_{\mathrm{M}}$) *is equivalent to the following problem:*

$$\min_{\mathbf{Q}\succeq 0,\mathbf{q},r} \; r + \left(\gamma_2 \boldsymbol{\Sigma} + \boldsymbol{\mu}\boldsymbol{\mu}^\top\right) \bullet \mathbf{Q} + \boldsymbol{\mu}^\top \mathbf{q} + \sqrt{\gamma_1} \left\| \boldsymbol{\Sigma}^{\frac{1}{2}} \left(\mathbf{q} + 2\mathbf{Q}\boldsymbol{\mu}\right) \right\|_2 \tag{$\mathcal{P}_{\mathrm{in}}$}$$

$$\text{s.t. } r \geq f\left(\mathbf{x},\boldsymbol{\xi}\right) - \boldsymbol{\xi}^\top \mathbf{Q} \boldsymbol{\xi} - \boldsymbol{\xi}^\top \mathbf{q}, \; \forall\, \boldsymbol{\xi} \in \Omega, \tag{12}$$

where $r \in \mathbb{R}$, $\mathbf{q} \in \mathbb{R}^{|\mathcal{M}|}$, *and* $\mathbf{Q} \in \mathbb{R}^{|\mathcal{M}|\times|\mathcal{M}|}$ *are dual variables associated with the three constraints in* $\mathcal{D}$.

Note that $f(\mathbf{x},\boldsymbol{\xi})$ in constraints (12) corresponds to the second-stage minimization problem ($\mathcal{P}_2$). Let $\max_{\pi\in\mathcal{Y}} \psi(\mathbf{x},\boldsymbol{\pi},\boldsymbol{\xi})$ denote the dual of the second-stage problem, where $\boldsymbol{\pi}$, $\psi(\cdot)$, and $\mathcal{Y}$ denote the vector of variables, objective function, and feasible region of the dual problem, respectively. Let $vert(\mathcal{Y})$ be a set of all vertices of the feasible region $\mathcal{Y}$ (see Appendix B for details). We replace $f(\mathbf{x},\boldsymbol{\xi})$ in (12) by the dual objective value $\psi(\mathbf{x},\boldsymbol{\pi},\boldsymbol{\xi})$ and obtain the following reformulation.

PROPOSITION 1. *Problem* ($\mathcal{P}_{\mathrm{in}}$) *is equivalent to*

$$\min_{\mathbf{Q}\succeq 0,\mathbf{q},r} \; r + \left(\gamma_2 \boldsymbol{\Sigma} + \boldsymbol{\mu}\boldsymbol{\mu}^\top\right) \bullet \mathbf{Q} + \boldsymbol{\mu}^\top \mathbf{q} + \sqrt{\gamma_1} \left\| \boldsymbol{\Sigma}^{\frac{1}{2}} \left(\mathbf{q} + 2\mathbf{Q}\boldsymbol{\mu}\right) \right\|_2 \tag{$\mathcal{P}'_{\mathrm{in}}$}$$

$$\text{s.t. } r \geq \psi\left(\mathbf{x},\boldsymbol{\pi},\boldsymbol{\xi}\right) - \boldsymbol{\xi}^\top \mathbf{Q} \boldsymbol{\xi} - \boldsymbol{\xi}^\top \mathbf{q}, \; \forall\, \boldsymbol{\xi} \in \Omega, \boldsymbol{\pi} \in vert\left(\mathcal{Y}\right). \tag{13}$$

We perform the above transformation to reduce the computational complexity. Recall that $f(\mathbf{x},\boldsymbol{\xi})$ is the optimal objective value of the minimization problem ($\mathcal{P}_2$). Since $f(\mathbf{x},\boldsymbol{\xi})$ is on the right-hand side of (12), we need to solve the minimization problem ($\mathcal{P}_2$) to *optimality*. In contrast, by considering the dual problem of ($\mathcal{P}_2$), we have a maximization problem on the right-hand side of (13). Since the dual problem is linear, its optimal solution must be one of the finite number of vertices of its feasible region. Therefore, we only need to *identify* a finite number of $\boldsymbol{\pi}$ (vertices) to ensure that constraints (13) hold.

It is still not straightforward to solve Problem ($\mathcal{P}'_{\mathrm{in}}$) because constraints (13) consider any $\boldsymbol{\xi}$ in Ω, which includes an infinite number of possible realizations. To overcome this challenge, we transform Problem ($\mathcal{P}'_{\mathrm{in}}$) to an SDP formulation and combine it with the outer minimization problem of ($\mathcal{P}_{\mathrm{M}}$). We rewrite $\psi(\mathbf{x},\boldsymbol{\pi},\boldsymbol{\xi})$ such that $\psi(\mathbf{x},\boldsymbol{\pi},\boldsymbol{\xi}) = \psi_1(\mathbf{x},\boldsymbol{\pi}) + \psi_2(\boldsymbol{\pi})^\top \boldsymbol{\xi}$ (see Appendix C for details). Proposition 2 presents the equivalent reformulation of Problem ($\mathcal{P}_{\mathrm{M}}$) that is solvable.

PROPOSITION 2. *Problem* $(\mathcal{P}_{\mathrm{M}})$ *is equivalent to*

$$\Gamma = \min_{\substack{\mathbf{x},\boldsymbol{\pi}\in vert(\mathcal{Y}) \\ \mathbf{Q}\succeq 0,\mathbf{q},r \\ \boldsymbol{\lambda}_1,\boldsymbol{\lambda}_2\geq \mathbf{0}}} \sum_{z\in\mathcal{Z}}\sum_{s\in\mathcal{S}} c_s x_{z,s} + r + \left(\gamma_2\boldsymbol{\Sigma} + \boldsymbol{\mu}\boldsymbol{\mu}^\top\right) \bullet \mathbf{Q} + \boldsymbol{\mu}^\top\mathbf{q} + \sqrt{\gamma_1}\left\|\boldsymbol{\Sigma}^{\frac{1}{2}}\left(\mathbf{q}+2\mathbf{Q}\boldsymbol{\mu}\right)\right\|_2 \qquad (\mathcal{P}_{\mathrm{F}})$$

$$\text{s.t. } (1)-(2),$$

$$\begin{bmatrix} r-\psi_1(\mathbf{x},\boldsymbol{\pi}) - \boldsymbol{\lambda}_1^\top\mathbf{b}^{\mathrm{ub}} + \boldsymbol{\lambda}_2^\top\mathbf{b}^{\mathrm{lb}} & \frac{1}{2}\left(\mathbf{q}+\mathbf{A}^\top(\boldsymbol{\lambda}_1-\boldsymbol{\lambda}_2)-\psi_2(\boldsymbol{\pi})\right)^\top \\ \frac{1}{2}\left(\mathbf{q}+\mathbf{A}^\top(\boldsymbol{\lambda}_1-\boldsymbol{\lambda}_2)-\psi_2(\boldsymbol{\pi})\right) & \mathbf{Q} \end{bmatrix} \succeq 0.$$

In summary, since Problem $(\mathcal{P}_{\mathrm{M}})$ is intractable, we first transform the inner max-min problem $\max_{\mathbb{P}\in\mathcal{D}} \mathbb{E}_{\mathbb{P}}[f(\mathbf{x},\boldsymbol{\xi})]$ of $(\mathcal{P}_{\mathrm{M}})$ to Problem $(\mathcal{P}_{\mathrm{in}})$, which is a minimization problem. After that, we find the dual of the minimization problem associated with $f(\mathbf{x},\boldsymbol{\xi})$ in constraints (12), and substitute $f(\mathbf{x},\boldsymbol{\xi})$ with its dual objective value to obtain a new problem $(\mathcal{P}'_{\mathrm{in}})$. We then transform $(\mathcal{P}'_{\mathrm{in}})$ to an SDP problem, and subsequently combine it with the outer minimization problem of $(\mathcal{P}_{\mathrm{M}})$, leading to Problem $(\mathcal{P}_{\mathrm{F}})$, which can be solved by off-the-shelf solvers such as Mosek.

5. Impact of Trip-Demand Correlations

The covariance matrix $\boldsymbol{\Sigma}$ in the ambiguity set (11) plays a critical role in solving Problem $(\mathcal{P}_{\mathrm{M}})$. In this section, we discuss the impact of the covariance matrix $\boldsymbol{\Sigma}$, which characterizes trip-demand correlations. Section 5.1 shows that the optimal total cost Γ of $(\mathcal{P}_{\mathrm{M}})$ is monotonic in the covariance matrix $\boldsymbol{\Sigma}$. We also identify the upper and lower bounds on the optimal total cost. Furthermore, the correlations of different pairs of trip demands, represented by the different entries of $\boldsymbol{\Sigma}$, may have different impact on the optimal total cost Γ. Section 5.2 determines the impact of the different entries of $\boldsymbol{\Sigma}$. Based on this impact, we can prioritize the different trip-demand pairs.

5.1. How The Optimal Total Cost Depends on The Covariance Matrix $\boldsymbol{\Sigma}$

Problem $(\mathcal{P}_{\mathrm{M}})$ considers the worst-case distribution within the ambiguity set $\mathcal{D}$, which is constructed based on a given covariance matrix $\boldsymbol{\Sigma}$. Therefore, the optimal total cost of $(\mathcal{P}_{\mathrm{M}})$ depends on the covariance matrix $\boldsymbol{\Sigma}$. Let $\Gamma(\boldsymbol{\Sigma})$ denote the optimal total cost of $(\mathcal{P}_{\mathrm{M}})$ for any given $\boldsymbol{\Sigma}\succeq 0$. Proposition 3 shows how the optimal total cost $\Gamma(\boldsymbol{\Sigma})$ changes with $\boldsymbol{\Sigma}$.

PROPOSITION 3. *Given two covariance matrices* $\boldsymbol{\Sigma}'', \boldsymbol{\Sigma}' \succeq 0$, *if* $\boldsymbol{\Sigma}'' \succeq \boldsymbol{\Sigma}'$, *then* $\Gamma(\boldsymbol{\Sigma}'') \geq \Gamma(\boldsymbol{\Sigma}')$.

Proposition 3 shows a monotonic relationship between the optimal total cost and $\boldsymbol{\Sigma}$, indicating that stronger trip-demand correlations lead to a higher optimal total cost for the operator. This is because stronger trip-demand correlations result in a more conservative solution, which has a higher total cost.

In practice, the operator can use realized samples $\hat{\boldsymbol{\xi}}_1,\ldots,\hat{\boldsymbol{\xi}}_N$ to estimate $\boldsymbol{\Sigma}$. That is, $\boldsymbol{\Sigma} = N^{-1}\sum_{n=1}^{N}(\hat{\boldsymbol{\xi}}_n-\boldsymbol{\mu})(\hat{\boldsymbol{\xi}}_n-\boldsymbol{\mu})^\top$. Note that this method of estimating $\boldsymbol{\Sigma}$ is inappropriate if N is small,

because $\mathbf{\Sigma}$ is high-dimensional and requires a substantial number of samples for accurate estimation. In this case, the operator may, instead, choose not to estimate $\mathbf{\Sigma}$ and neglect the third set of constraints in (11), resulting in the following model:

$$\overline{\Gamma} = \min_{\mathbf{x}} \left\{ \sum_{z\in\mathcal{Z}} \sum_{s\in\mathcal{S}} c_s x_{z,s} + \max_{\mathbb{P}\in\mathcal{D}_1} \mathbb{E}_{\mathbb{P}} \left[f\left(\mathbf{x}, \boldsymbol{\xi}\right) \right] \;\middle|\; (1)-(2) \right\}, \tag{14}$$

where $\mathcal{D}_1(\Omega, \boldsymbol{\mu}, \gamma_1) = \{\mathbb{P} \mid \mathbb{P}(\boldsymbol{\xi} \in \Omega) = 1, (\mathbb{E}_{\mathbb{P}}[\boldsymbol{\xi}] - \boldsymbol{\mu})^\top \mathbf{\Sigma}^{-1} (\mathbb{E}_{\mathbb{P}}[\boldsymbol{\xi}] - \boldsymbol{\mu}) \leq \gamma_1\}$. As $\mathcal{D}_1$ ignores constraints on the covariance matrix, Problem (14) considers all possible trip-demand correlations, including both zero and strong correlations. This makes the ambiguity set $\mathcal{D}_1$ include more distributions than $\mathcal{D}$ in (11). Consequently, Problem (14) has a larger optimal total cost than Problem ($\mathcal{P}_{\mathrm{M}}$) as shown in Proposition 4.

PROPOSITION 4. *Given the optimal cost* $\overline{\Gamma}$ *of Problem* (14)*, we have* $\Gamma(\mathbf{\Sigma}) \leq \overline{\Gamma}$ *for any* $\mathbf{\Sigma} \succeq 0$*.*

Proposition 4 provides an upper bound on the optimal total cost of ($\mathcal{P}_{\mathrm{M}}$) with any covariance matrix $\mathbf{\Sigma}$. This implies that although a larger covariance matrix $\mathbf{\Sigma}$ leads to a larger optimal total cost of ($\mathcal{P}_{\mathrm{M}}$) as shown in Proposition 3, its impact is upper-bounded. Moreover, Proposition 4 provides the operator with the most conservative estimation of the optimal total cost even if the operator has no knowledge about trip-demand correlations. This facilitates the operator's decision-making.

Let $\mathbf{\Sigma}_{i,j}$ denote the (i,j)th entry of matrix $\mathbf{\Sigma}$ for any $i, j \in \{1, \ldots, |\mathcal{M}|\}$. Proposition 5 provides a lower bound on the optimal total cost of ($\mathcal{P}_{\mathrm{M}}$).

PROPOSITION 5. *For any* $\mathbf{\Sigma} \succeq 0$ *that satisfies* $\sum_{j\in\{1,\ldots,|\mathcal{M}|\}, j\neq i} |\mathbf{\Sigma}_{i,j}| < \mathbf{\Sigma}_{i,i}$ *for all* $i \in \{1, \ldots, |\mathcal{M}|\}$*, there exists a diagonal matrix* $\mathbf{\Sigma}^{\mathrm{d}} \succeq 0$ *and* $\mathbf{\Sigma}^{\mathrm{d}} \neq \mathbf{0}$*, such that* $\Gamma(\mathbf{\Sigma}^{\mathrm{d}}) \leq \Gamma(\mathbf{\Sigma})$*.*

Proposition 5 shows that if the operator is confident that the degree of covariance among trip demands (the sum of off-diagonal entries in each row of $\mathbf{\Sigma}$) is low, it may be in the operator's interest to assume all trip demands are independent, leading to an optimistic solution that provides a lower bound on the optimal total cost of ($\mathcal{P}_{\mathrm{M}}$). However, even though assuming the independence among trip demands provides a lower bound on the optimal total cost, it does not guarantee a good performance in out-of-sample numerical experiments as will be seen in Section 7.3. We call this phenomenon the *danger of optimism*. To overcome this, we need to estimate some off-diagonal entries of $\mathbf{\Sigma}$ when solving ($\mathcal{P}_{\mathrm{M}}$). Section 5.2 tells us which off-diagonal entries to prioritize.

5.2. Which Trip-Demand Pairs Should Be Prioritized

To mitigate the danger of optimism, which results from assuming trip demands are independent, we need to estimate and include the covariance of trip demands. However, in practice, the operator has limited resources and is able to quantify correlations between only selected trip-demand

pairs, rather than all pairs. Therefore, it is crucial to prioritize the trip-demand pairs to ensure good performance when solving Problem ($\mathcal{P}_{\mathrm{M}}$).

Intuitively, the operator can prioritize the trip-demand pairs that have high correlations. For example, as suggested by Figures 1 and 2, trips during morning and evening rush hours, as well as those in office and residence regions, are highly correlated. Additionally, trips tend to show stronger correlations in space than in time. Based on these observations, the operator may aim to measure the correlations between trip demands in office and residence regions, while assuming that other trip demands remain independent.

Alternatively, when choosing which trip-demand pairs to include to solve ($\mathcal{P}_{\mathrm{M}}$), the shadow prices of covariance constraints $\mathbb{E}_{\mathbb{P}}[(\boldsymbol{\xi}-\boldsymbol{\mu})(\boldsymbol{\xi}-\boldsymbol{\mu})^{\top}] \preceq \gamma_2 \boldsymbol{\Sigma}$ in (11), can also offer valuable insights. Each shadow price represents the impact of an increase in the covariance of a trip-demand pair on the objective function value. A higher shadow price signifies a greater impact of the corresponding trip-demand pair. Based on the shadow prices, the operator can identify which trip-demand pairs have a significant impact on the total cost and then prioritize them. Proposition 6 determines the shadow price of each trip-demand pair. Recall that $\mathbf{Q} \in \mathbb{R}^{|\mathcal{M}|\times|\mathcal{M}|}$ are the dual variables of the covariance constraints $\mathbb{E}_{\mathbb{P}}[(\boldsymbol{\xi}-\boldsymbol{\mu})(\boldsymbol{\xi}-\boldsymbol{\mu})^{\top}] \preceq \gamma_2 \boldsymbol{\Sigma}$.

PROPOSITION 6. *Given any allocation solution* $\mathbf{x}$*, let* $\mathbb{P}^*$ *represent the optimal distribution of the inner maximization problem of* ($\mathcal{P}_{\mathrm{M}}$)*,* $\mathrm{supp}(\mathbb{P}^*)$ *represent the support set associated with* $\mathbb{P}^*$*, and* $\mathbf{Q}^*$ *represent the optimal value of* $\mathbf{Q}$*. For any* $i, j \in \{1,\ldots,|\mathcal{M}|\}, i \neq j$*, if there exist* $\boldsymbol{\xi} \in \mathrm{supp}(\mathbb{P}^*)$ *and* $\delta_i, \delta_j \in \mathbb{R}$ *such that* $\boldsymbol{\xi}+\delta_i\mathbf{e}_i, \boldsymbol{\xi}+\delta_j\mathbf{e}_j, \boldsymbol{\xi}+\delta_j\mathbf{e}_j+\delta_i\mathbf{e}_i \in \mathrm{supp}(\mathbb{P}^*)$*, where* $\mathbf{e}_i$ *and* $\mathbf{e}_j$ *are unit vectors, we have*

$$\mathbf{Q}^*_{i,j} = \frac{(f(\mathbf{x},\boldsymbol{\xi}) - f(\mathbf{x},\boldsymbol{\xi}+\delta_i\mathbf{e}_i)) - (f(\mathbf{x},\boldsymbol{\xi}+\delta_j\mathbf{e}_j) - f(\mathbf{x},\boldsymbol{\xi}+\delta_j\mathbf{e}_j+\delta_i\mathbf{e}_i))}{2\delta_i\delta_j}. \tag{15}$$

We obtain Equation (15) because the optimal dual variables $\mathbf{Q}^*$ satisfy the complementary conditions. Proposition 6 quantifies the shadow prices of the covariance constraints, which depends on the second-stage optimal cost f with the uncertainty changes in the directions of trip i, trip j, and both, for $i, j \in \{1,\ldots,|\mathcal{M}|\}, i \neq j$. Moreover, since the second-stage optimal cost $f(\mathbf{x},\boldsymbol{\xi})$ depends on the allocation decision $\mathbf{x}$, by (15), we can conclude that the allocation decision influences the shadow prices of the covariance constraints, thereby affecting the impact of the correlations.

In addition to these theoretical findings regarding ($\mathcal{P}_{\mathrm{M}}$) and (14), Sections 7.3 and 7.4 examine their numerical results with real data, providing deeper insights into the impact of correlations.

6. Solution Approaches

Although we have converted Problem ($\mathcal{P}_{\mathrm{M}}$) to Problem ($\mathcal{P}_{\mathrm{F}}$) in Section 4. In practice, it is still very challenging to solve ($\mathcal{P}_{\mathrm{F}}$) directly using off-the-shelf solvers because the network $\mathcal{G}$ can be very large, which results in a high-dimensional PSD matrix and a large-size $vert(\mathcal{Y})$. In this section, we

first propose three approximation approaches to solve $(\mathcal{P}_{\mathrm{F}})$ more efficiently: (i) The first approach considers an outer approximation of $(\mathcal{P}_{\mathrm{F}})$ and provides a lower bound on its optimal objective value. (ii) The second approach considers an inner approximation of $(\mathcal{P}_{\mathrm{F}})$ and provides an upper bound on its optimal objective value. (iii) The third approach solves the problem by considering only a portion of $vert(\mathcal{Y})$. Based on the above three approaches, we develop a hybrid algorithm that first decomposes $\mathcal{G} = (\mathcal{N}, \mathcal{A})$ into L sub-networks along the operational horizon with each sub-network $l \in \{1, 2, \ldots, L\}$ having a shorter time horizon. We solve a sequence of smaller SDP problems, each corresponding to a sub-network, in a backward manner from the last sub-network to the first one. For each sub-network, we apply the three approaches sequentially. We first derive the outer approximation of the sub-problem. Based on this approximation, we then derive its inner approximation, which is subsequently solved using the third approach. We will use this hybrid algorithm to solve the DRO model in the numerical experiments in Section 7.

Before introducing the outer and inner approximations of $(\mathcal{P}_{\mathrm{F}})$, we first reformulate Problem $(\mathcal{P}_{\mathrm{M}})$ as follows. We perform an eigenvalue decomposition on the covariance matrix $\mathbf{\Sigma} = \mathbf{U}\mathbf{\Lambda}\mathbf{U}^{\top} = \mathbf{U}\mathbf{\Lambda}^{1/2}(\mathbf{U}\mathbf{\Lambda}^{1/2})^{\top}$. Here, $\mathbf{U} \in \mathbb{R}^{|\mathcal{M}|\times|\mathcal{M}|}$ is an orthogonal transformation matrix and $\mathbf{\Lambda} \in \mathbb{R}^{|\mathcal{M}|\times|\mathcal{M}|}$ is a diagonal matrix with diagonal elements in a decreasing order. By letting $\boldsymbol{\xi}_{\mathrm{I}} = (\mathbf{U}\mathbf{\Lambda}^{-1/2})^{\top}(\boldsymbol{\xi} - \boldsymbol{\mu})$, we reformulate Problem $(\mathcal{P}_{\mathrm{M}})$ as

$$\Gamma = \min_{\mathbf{x}} \left\{ \sum_{z\in\mathcal{Z}} \sum_{s\in\mathcal{S}} c_s x_{z,s} + \max_{\mathbb{P}_{\mathrm{I}}\in\mathcal{D}_{\mathrm{I}}} \mathbb{E}_{\mathbb{P}_{\mathrm{I}}} \left[f\left(\mathbf{x}, \mathbf{U}\mathbf{\Lambda}^{1/2}\boldsymbol{\xi}_{\mathrm{I}} + \boldsymbol{\mu}\right) \right] \,\middle|\, (1)-(2) \right\}, \tag{$\mathcal{P}_{\mathrm{I}}$}$$

where

$$\mathcal{D}_{\mathrm{I}}\left(\Omega_{\mathrm{I}}, \gamma_1, \gamma_2\right) = \left\{ \mathbb{P}_{\mathrm{I}} \middle| \begin{array}{l} \mathbb{P}_{\mathrm{I}}\left(\boldsymbol{\xi}_{\mathrm{I}} \in \Omega_{\mathrm{I}}\right) = 1 \\ \mathbb{E}_{\mathbb{P}_{\mathrm{I}}}\left[\boldsymbol{\xi}_{\mathrm{I}}^{\top}\right] \mathbb{E}_{\mathbb{P}_{\mathrm{I}}}\left[\boldsymbol{\xi}_{\mathrm{I}}\right] \leq \gamma_1 \\ \mathbb{E}_{\mathbb{P}_{\mathrm{I}}}\left[\boldsymbol{\xi}_{\mathrm{I}}\boldsymbol{\xi}_{\mathrm{I}}^{\top}\right] \preceq \gamma_2 \mathbf{I}_{|\mathcal{M}|} \end{array} \right\},$$

with $\Omega_{\mathrm{I}} := \{\boldsymbol{\xi}_{\mathrm{I}} \in \mathbb{R}^{|\mathcal{M}|} \mid \mathbf{U}\mathbf{\Lambda}^{1/2}\boldsymbol{\xi}_{\mathrm{I}} + \boldsymbol{\mu} \in \Omega\}$ and $\mathbf{I}_{|\mathcal{M}|}$ denoting an identity matrix of size $|\mathcal{M}| \times |\mathcal{M}|$. We will construct the outer and inner approximations of the DRO model $(\mathcal{P}_{\mathrm{F}})$ (or, equivalently, $(\mathcal{P}_{\mathrm{M}})$) based on Problem $(\mathcal{P}_{\mathrm{I}})$.

6.1. Approach 1: Outer Approximation of DRO Model

We use principal component analysis (PCA) (Cheramin et al. 2022), which approximates a high-dimensional matrix with a low-dimensional one, to reduce the size of the DRO model while maintaining a high solution quality. We approximate $\boldsymbol{\xi}$ by capturing the main variability of $\mathbf{U}\mathbf{\Lambda}^{1/2}\boldsymbol{\xi}_{\mathrm{I}}$ by considering $\boldsymbol{\xi}_m \in \mathbb{R}^m$, which denotes a vector containing the first m entries of $\boldsymbol{\xi}_{\mathrm{I}}$. Specifically, we approximate

$$\boldsymbol{\xi} = \mathbf{U}\mathbf{\Lambda}^{\frac{1}{2}}\boldsymbol{\xi}_{\mathrm{I}} + \boldsymbol{\mu} \approx \mathbf{U}\mathbf{\Lambda}^{\frac{1}{2}}[\boldsymbol{\xi}_m; \mathbf{0}_{|\mathcal{M}|-m}] + \boldsymbol{\mu} = \mathbf{U}_{|\mathcal{M}|\times m}\mathbf{\Lambda}_m^{\frac{1}{2}}\boldsymbol{\xi}_m + \boldsymbol{\mu},$$

where $\mathbf{0}_{|\mathcal{M}|-m}$ represents a zero vector of size $|\mathcal{M}|-m$, $\mathbf{U}_{|\mathcal{M}|\times m} \in \mathbb{R}^{|\mathcal{M}|\times m}$ and $\mathbf{\Lambda}_m^{1/2} \in \mathbb{R}^{m\times m}$ are upper-left submatrices of $\mathbf{U}$ and $\mathbf{\Lambda}^{1/2}$, respectively. By neglecting the last $|\mathcal{M}|-m$ entries of $\boldsymbol{\xi}_{\mathrm{I}}$, we have a relaxation of Problem $(\mathcal{P}_{\mathrm{M}})$ as follows, called the *outer approximation* of the DRO model:

$$\min_{\mathbf{x}} \left\{ \sum_{z\in\mathcal{Z}} \sum_{s\in\mathcal{S}} c_s x_{z,s} + \max_{\mathbb{P}_m\in\mathcal{D}_m} \mathbb{E}_{\mathbb{P}_m}\left[f\left(\mathbf{x}, \mathbf{U}_{|\mathcal{M}|\times m}\mathbf{\Lambda}_m^{\frac{1}{2}}\boldsymbol{\xi}_m + \boldsymbol{\mu}\right)\right] \,\middle|\, (1)-(2) \right\}, \tag{16}$$

where

$$\mathcal{D}_m\left(\Omega_m, \gamma_1, \gamma_2\right) = \left\{ \mathbb{P}_m \,\middle|\, \begin{array}{l} \mathbb{P}_m\left(\boldsymbol{\xi}_m \in \Omega_m\right) = 1 \\ \mathbb{E}_{\mathbb{P}_m}\left[\boldsymbol{\xi}_m^\top\right]\mathbb{E}_{\mathbb{P}_m}\left[\boldsymbol{\xi}_m\right] \le \gamma_1 \\ \mathbb{E}_{\mathbb{P}_m}\left[\boldsymbol{\xi}_m\boldsymbol{\xi}_m^\top\right] \preceq \gamma_2 \mathbf{I}_m \end{array} \right\},$$

with $\Omega_m := \{\boldsymbol{\xi}_m \in \mathbb{R}^m : \mathbf{U}_{|\mathcal{M}|\times m}\mathbf{\Lambda}_m^{1/2}\boldsymbol{\xi}_m + \boldsymbol{\mu} \in \Omega\}$.

We adopt the same sequence of reformulations in Section 4 to transform Problem (16) into a solvable model.

THEOREM 2. *Problem* (16) *has the same optimal objective value as the following problem:*

$$\begin{aligned} \min_{\mathbf{x},\mathbf{Q}_m,\mathbf{q}_m,r} \; & \sum_{z\in\mathcal{Z}}\sum_{s\in\mathcal{S}} c_s x_{z,s} + r + \gamma_2 I_m \bullet \mathbf{Q}_m + \sqrt{\gamma_1}\|\mathbf{q}_m\|_2 \\ \text{s.t. } & (1)-(2), \\ & r \ge f\left(\mathbf{x}, \mathbf{U}_{|\mathcal{M}|\times m}\mathbf{\Lambda}_m^{\frac{1}{2}}\boldsymbol{\xi}_m + \boldsymbol{\mu}\right) - \boldsymbol{\xi}_m^\top\mathbf{Q}_m\boldsymbol{\xi}_m - \boldsymbol{\xi}_m^\top\mathbf{q}_m, \; \forall\, \boldsymbol{\xi}_m \in \Omega_m, \\ & \mathbf{Q}_m \succeq 0, \end{aligned} \tag{17}$$

where $\mathbf{Q}_m \in \mathbb{R}^{m\times m}$ *and* $\mathbf{q}_m \in \mathbb{R}^m$. *Furthermore, the following results hold: (i) Problem* (17) *provides a lower bound on the optimal objective value of* $(\mathcal{P}_{\mathrm{M}})$*; (ii) the optimal objective value of* (17) *is nondecreasing in* m*; and (iii) if* $m = |\mathcal{M}|$*, then Problems* (17) *and* $(\mathcal{P}_{\mathrm{M}})$ *have the same optimal objective value.*

PROPOSITION 7. *Problem* (17) *has the same optimal objective value as the following SDP model:*

$$\begin{aligned} \min_{\substack{\mathbf{x},\boldsymbol{\pi}\in vert(\mathcal{Y}) \\ \mathbf{Q}_m\succeq 0,\mathbf{q}_m,r \\ \boldsymbol{\lambda}_1,\boldsymbol{\lambda}_2\ge\mathbf{0}}} \; & \sum_{z\in\mathcal{Z}}\sum_{s\in\mathcal{S}} c_s x_{z,s} + r + \gamma_2 I_m \bullet \mathbf{Q}_m + \sqrt{\gamma_1}\|\mathbf{q}_m\|_2 \\ \text{s.t. } & (1)-(2), \\ & \begin{bmatrix} \mathbf{M}_1 & \mathbf{M}_2^\top \\ \mathbf{M}_2 & \mathbf{Q}_m \end{bmatrix} \succeq 0, \end{aligned} \tag{18}$$

where $\mathbf{M}_1 = r - \psi_1(\mathbf{x},\boldsymbol{\pi}) - \boldsymbol{\lambda}_1^\top\mathbf{b}^{\mathrm{ub}} + \boldsymbol{\lambda}_2^\top\mathbf{b}^{\mathrm{lb}} - \psi_2(\boldsymbol{\pi})^\top\boldsymbol{\mu} + (\boldsymbol{\lambda}_1-\boldsymbol{\lambda}_2)^\top\mathbf{A}\boldsymbol{\mu}$ *and* $\mathbf{M}_2 = (1/2)\times(\mathbf{q}_m + (\mathbf{U}_{|\mathcal{M}|\times m}\mathbf{\Lambda}_m^{1/2})^\top(\mathbf{A}^\top(\boldsymbol{\lambda}_1-\boldsymbol{\lambda}_2) - \psi_2(\boldsymbol{\pi})))$.

It is worth noting that Problem (18) is significantly easier to solve than $(\mathcal{P}_{\mathrm{F}})$ because the PSD matrix in (18) is significantly smaller than that in $(\mathcal{P}_{\mathrm{F}})$ (i.e., the matrix dimensions are $(m+1)\times(m+1)$ versus $(|\mathcal{M}|+1)\times(|\mathcal{M}|+1)$).

6.2. Approach 2: Inner Approximation of DRO Model

To reduce the size of the PSD matrix in ($\mathcal{P}_{\mathrm{F}}$), we split the random vector $\boldsymbol{\xi}_{\mathrm{I}}$ into several pieces. Specifically, we split $\boldsymbol{\xi}_{\mathrm{I}}$ into U pieces, i.e., $\boldsymbol{\xi}_{\mathrm{I}} = (\boldsymbol{\xi}_{\mathrm{I}_1}^\top, \boldsymbol{\xi}_{\mathrm{I}_2}^\top, \ldots, \boldsymbol{\xi}_{\mathrm{I}_U}^\top)^\top$, where $\boldsymbol{\xi}_{\mathrm{I}_i} \in \mathbb{R}^{m_i}$, $i \in \{1, \ldots, U\}$, and $\sum_{i=1}^{U} m_i = |\mathcal{M}|$. Accordingly, we approximate the second-moment constraint in $\mathcal{D}_{\mathrm{I}}$ using these smaller pieces, leading to the following ambiguity set:

$$\mathcal{D}_{\mathrm{U}}(\Omega_{\mathrm{I}}, \gamma_1, \gamma_2) = \left\{ \mathbb{P}_{\mathrm{U}} \left| \begin{array}{l} \mathbb{P}_{\mathrm{U}}(\boldsymbol{\xi}_{\mathrm{I}} \in \Omega_{\mathrm{I}}) = 1 \\ \mathbb{E}_{\mathbb{P}_{\mathrm{U}}}[\boldsymbol{\xi}_{\mathrm{I}}^\top]\, \mathbb{E}_{\mathbb{P}_{\mathrm{U}}}[\boldsymbol{\xi}_{\mathrm{I}}] \leq \gamma_1 \\ \mathbb{E}_{\mathbb{P}_{\mathrm{U}}}\left[\boldsymbol{\xi}_{\mathrm{I}_i} \boldsymbol{\xi}_{\mathrm{I}_i}^\top\right] \preceq \gamma_2 \mathbf{I}_{m_i},\ \forall i \in \{1, \ldots, U\} \end{array} \right. \right\}.$$

The set $\mathcal{D}_{\mathrm{U}}$ is a superset of $\mathcal{D}_{\mathrm{I}}$ because we ignore the correlations among $\boldsymbol{\xi}_{\mathrm{I}_i}$ and $\boldsymbol{\xi}_{\mathrm{I}_j}$ for any $i, j \in \{1, \ldots, U\}, i \neq j$. This leads to the following approximation of Problem ($\mathcal{P}_{\mathrm{M}}$), called the *inner approximation* of the DRO model:

$$\min_{\mathbf{x}} \left\{ \sum_{z \in \mathcal{Z}} \sum_{s \in \mathcal{S}} c_s x_{z,s} + \max_{\mathbb{P}_{\mathrm{U}} \in \mathcal{D}_{\mathrm{U}}} \mathbb{E}_{\mathbb{P}_{\mathrm{U}}} \left[f\left(\mathbf{x}, \mathbf{U}\boldsymbol{\Lambda}^{\frac{1}{2}} \boldsymbol{\xi}_{\mathrm{I}} + \boldsymbol{\mu}\right) \right] \,\middle|\, (1) - (2) \right\}. \tag{19}$$

Similarly, we adopt the same reformulation sequence in Section 4 to transform Problem (19) into a solvable model.

THEOREM 3. *Problem* (19) *has the same optimal objective value as the following problem:*

$$\begin{aligned} \min_{\mathbf{x}, \mathbf{Q}_i, \mathbf{q}, r} \ & \sum_{z \in \mathcal{Z}} \sum_{s \in \mathcal{S}} c_s x_{z,s} + r + \gamma_2 \sum_{i=1}^{U} I_{m_i} \bullet \mathbf{Q}_i + \sqrt{\gamma_1} \|\mathbf{q}\|_2 \\ \text{s.t. } & (1) - (2), \\ & r \geq f\left(\mathbf{x}, \mathbf{U}\boldsymbol{\Lambda}^{\frac{1}{2}} \boldsymbol{\xi}_{\mathrm{I}} + \boldsymbol{\mu}\right) - \sum_{i=1}^{U} \boldsymbol{\xi}_{\mathrm{I}_i}^\top \mathbf{Q}_i \boldsymbol{\xi}_{\mathrm{I}_i} - \boldsymbol{\xi}_{\mathrm{I}}^\top \mathbf{q},\ \forall \boldsymbol{\xi}_{\mathrm{I}} \in \Omega_{\mathrm{I}}, \\ & \mathbf{Q}_i \succeq 0,\ \forall i \in \{1, \ldots, U\}, \end{aligned} \tag{20}$$

where $\mathbf{Q}_i \in \mathbb{R}^{m_i \times m_i}$, $i \in \{1, \ldots, U\}$, *and* $\mathbf{q} \in \mathbb{R}^{|\mathcal{M}|}$. *Furthermore, Problem* (20) *provides an upper bound on the optimal objective value of Problem* ($\mathcal{P}_{\mathrm{M}}$).

PROPOSITION 8. *Problem* (20) *has the same optimal objective value as the following SDP model:*

$$\begin{aligned} \min_{\substack{\mathbf{x}, \boldsymbol{\pi} \in vert(\mathcal{Y}) \\ \mathbf{Q}_i, \mathbf{q}_i, \mathbf{q}, r_i, r \\ \boldsymbol{\lambda}_1, \boldsymbol{\lambda}_2 \geq \mathbf{0}}} \ & \sum_{z \in \mathcal{Z}} \sum_{s \in \mathcal{S}} c_s x_{z,s} + r + \gamma_2 \sum_{i=1}^{U} I_{m_i} \bullet \mathbf{Q}_i + \sqrt{\gamma_1} \|\mathbf{q}\|_2 \\ \text{s.t. } & (1) - (2), \\ & \begin{bmatrix} r_i & \mathbf{M}_2^{i\top} \\ \mathbf{M}_2^i & \mathbf{Q}_i \end{bmatrix} \succeq 0,\ \forall i \in \{1, \ldots, U\}, \\ & \sum_{i=1}^{U} r_i = r - \psi_1(\mathbf{x}, \boldsymbol{\pi}) - \boldsymbol{\lambda}_1^\top \mathbf{b}^{\mathrm{ub}} + \boldsymbol{\lambda}_2^\top \mathbf{b}^{\mathrm{lb}} - \psi_2(\boldsymbol{\pi})^\top \boldsymbol{\mu} + (\boldsymbol{\lambda}_1 - \boldsymbol{\lambda}_2)^\top \mathbf{A}\boldsymbol{\mu}, \\ & \mathbf{Q}_i \succeq 0,\ \forall i \in \{1, \ldots, U\}, \end{aligned} \tag{21}$$

where $\mathbf{M}_2^i = 1/2 \times (\mathbf{q}_i + (\mathbf{U}_{|\mathcal{M}| \times m_i} \boldsymbol{\Lambda}_{m_i}^{1/2})^\top (\mathbf{A}^\top (\boldsymbol{\lambda}_1 - \boldsymbol{\lambda}_2) - \psi_2(\boldsymbol{\pi})))$, $\mathbf{q}_i \in \mathbb{R}^{m_i}$, $\mathbf{q} = (\mathbf{q}_1^\top, \ldots, \mathbf{q}_U^\top)^\top$, *and* $\mathbf{Q}_i \in \mathbb{R}^{m_i \times m_i}$ *for any* $i \in \{1, \ldots, U\}$.

Again, Problem (21) is significantly easier to solve than ($\mathcal{P}_{\mathrm{F}}$) because the PSD matrices in (21) are significantly smaller.

6.3. Approach 3: Delayed Constraint Generation Algorithm

It is not practical to enumerate all vertices of the feasible region in $vert(\mathcal{Y})$ for Problems ($\mathcal{P}_{\mathrm{F}}$), (18), and (21). To overcome this challenge, we use the Delayed Constraint Generation Algorithm by Fathabad et al. (2020), which solves the problem by considering a subset of vertices $\mathcal{V}_{\mathrm{r}} \subseteq vert(\mathcal{Y})$. Algorithm 1 presents an adapted version of this algorithm for Problem ($\mathcal{P}_{\mathrm{F}}$). Similar algorithms can be developed to solve Problems (18) and (21).

Algorithm 1 Delayed Constraint Generation Algorithm

1: Find some initial vertex of the feasible region $\mathcal{Y}$, denoted by $\boldsymbol{\pi}^*$. Set $\mathcal{V}_{\mathrm{r}} = \emptyset$.
2: **do**
3: $\quad \mathcal{V}_{\mathrm{r}} = \mathcal{V}_{\mathrm{r}} \cup \{\boldsymbol{\pi}^*\}$.
4: $\quad$ Solve Problem ($\mathcal{P}_{\mathrm{F}}$) considering the vertices only in $\mathcal{V}_{\mathrm{r}}$. Then, save the optimal objective value Γ^* and optimal solution $(\mathbf{x}^*, \mathbf{Q}^*, \mathbf{q}^*, r^*)$.
5: $\quad$ Solve the following biconvex problem using $(\mathbf{x}^*, \mathbf{Q}^*, \mathbf{q}^*, r^*)$:

$$\min_{\boldsymbol{\pi} \in \mathcal{Y},\, \boldsymbol{\xi} \in \Omega} \; r^* + \boldsymbol{\xi}^\top \mathbf{Q}^* \boldsymbol{\xi} + \boldsymbol{\xi}^\top \mathbf{q}^* - \psi\left(\mathbf{x}^*, \boldsymbol{\pi}, \boldsymbol{\xi}\right), \tag{22}$$

$\quad$ and save the optimal objective value as s^* and optimal solution as $\boldsymbol{\pi}^*$.
6: **while** $s^* < 0$
7: Return Γ^* and $\mathbf{x}^*$.

Algorithm 1 initially solves a relaxation of the SDP problem by considering $\mathcal{V}_{\mathrm{r}}$ that is significantly smaller than $vert(\mathcal{Y})$. Before converging, it iteratively adds vertices of $\mathcal{Y}$ to the subset $\mathcal{V}_{\mathrm{r}}$ and solves the SDP problem. Note that at the beginning, we obtain some initial vertex of $\mathcal{Y}$ by solving a linear programming problem subject to $\mathcal{Y}$. Problem (22) is nonlinear because of the bilinear terms in $\psi(\mathbf{x}^*, \boldsymbol{\pi}, \boldsymbol{\xi})$ (see Appendix B for details). We can solve this problem to a near-optimal solution by using the alternating direction search algorithm or alternating direction method of multipliers (ADMM) (Fathabad et al. 2020).

6.4. Hybrid Algorithm

Algorithm 1 solves Problem ($\mathcal{P}_{\mathrm{F}}$) with $\mathcal{V}_{\mathrm{r}}$ iteratively. Even though $\mathcal{V}_{\mathrm{r}}$ is significantly smaller than $vert(\mathcal{Y})$, it is still computationally expensive to solve ($\mathcal{P}_{\mathrm{F}}$) because of a large number of variables and constraints induced by a large network $\mathcal{G} = (\mathcal{N}, \mathcal{A})$. We thus adopt a temporal decomposition approach together with the three approaches above to iteratively solve a sequence of sub-problems, each of which considers only a part of $\mathcal{G}$. Specifically, we decompose $\mathcal{G}$ into L sub-networks, each sub-network $l \in \{1, 2, \ldots, L\}$ has a time horizon with T_l periods, where $\sum_{l=1}^{L} T_l = T$. For notational convenience, let $\mathcal{T}_1 = \{0, \ldots, T_1\}$ and $\mathcal{T}_l = \{\sum_{i=1}^{l-1} T_i + 1, \ldots, \sum_{i=1}^{l} T_i\}$, $l \in \{2, \ldots, L\}$. Likewise, for $l \in \{1, \ldots, L\}$, define $\mathcal{N}_l = \{n_{z,t,s} \in \mathcal{N} | z \in \mathcal{Z}, t \in \mathcal{T}_l, s \in \mathcal{S}\}$, $\mathcal{A}_l = \{(n_{z,t,s}, n_{z',t',s'}) \in \mathcal{A} | n_{z,t,s}, n_{z',t',s'} \in \mathcal{N}_l\}$, and $\mathcal{G}_l = (\mathcal{N}_l, \mathcal{A}_l)$. For sub-network $\mathcal{G}_l$, $l \in \{1, \ldots, L\}$, we denote the corresponding ($\mathcal{P}_{\mathrm{F}}$) as ($\mathcal{P}_{\mathrm{F}}^l$) (see Appendix L for details).

Algorithm 2 Hybrid Algorithm

Input: L, m, U.
1: Derive the outer approximation of Problem $(\mathcal{P}_{\mathrm{F}}^{L})$ with dimension m, denoted by $(\mathcal{P}_{\mathrm{F}}^{L,m})$.
2: Derive the inner approximation of Problem $(\mathcal{P}_{\mathrm{F}}^{L,m})$ with U pieces, denoted by $(\mathcal{P}_{\mathrm{F}}^{L,m,U})$.
3: Use Algorithm 1 to solve Problem $(\mathcal{P}_{\mathrm{F}}^{L,m,U})$, and save its optimal allocation decisions as $\overline{\mathbf{x}}^{L}$.
4: **for** $l = L-1,\ldots,1$ **do**
5: Derive Problem $(\mathcal{P}_{\mathrm{F}}^{l,m,U})$.
6: Add constraints $\sum_{z\in\mathcal{Z}}\sum_{s\in\mathcal{S}} x_{z,s} \geq \sum_{z\in\mathcal{Z}}\sum_{s\in\mathcal{S}} \overline{x}_{z,s}^{l+1}$ to Problem $(\mathcal{P}_{\mathrm{F}}^{l,m,U})$.
7: Use Algorithm 1 to solve Problem $(\mathcal{P}_{\mathrm{F}}^{l,m,U})$. Save its optimal allocation decisions as $\overline{\mathbf{x}}^{l}$.
8: **end for**
Output: Return $\overline{\mathbf{x}}^{1}$.

In Algorithm 2, we solve a smaller SDP problem over each sub-network $l \in \{L, L-1,\ldots,1\}$ in a backward manner, from sub-network L to sub-network 1. In each iteration $l \in \{L-1,\ldots,1\}$, we add constraints $\sum_{z\in\mathcal{Z}}\sum_{s\in\mathcal{S}} x_{z,s} \geq \sum_{z\in\mathcal{Z}}\sum_{s\in\mathcal{S}} \overline{x}_{z,s}^{l+1}$ to Problem $(\mathcal{P}_{\mathrm{F}}^{l})$ such that the total initial allocation of sub-network l is lower-bounded by $\sum_{z\in\mathcal{Z}}\sum_{s\in\mathcal{S}} \overline{x}_{z,s}^{l+1}$. The intuition behind such constraints is due to (i) the vehicle allocation decisions for the SDP problem over sub-network l should approximate that over sub-networks l to L, (ii) the total trip demand over sub-networks l to L is no less than that over sub-networks $l+1$ to L, and (iii) a larger total trip demand often needs more EVs. Finally, we obtain $\overline{\mathbf{x}}^{1}$ for Problem $(\mathcal{P}_{\mathrm{F}})$. We will use Algorithm 2 to solve $(\mathcal{P}_{\mathrm{F}})$ in the numerical experiments in the following section.

7. Numerical Experiments Using Real Data

We conduct numerical experiments with real data of taxi trip demands in NYC. We first describe parameter settings and then obtain insights from various experiments based on these settings.

7.1. Setting The Parameters

We have collected trip data of NYC from TLC (2024) from January 1, 2014 to December 31, 2019. We use the data in 2014, 2016, and 2018 to compute $\boldsymbol{\mu}$ and $\boldsymbol{\Sigma}$ for constructing the ambiguity set $\mathcal{D}$, and then solve $(\mathcal{P}_{\mathrm{M}})$ to obtain the first-stage solution $\mathbf{x}$. Using the data in 2015, 2017, and 2019, we then perform out-of-sample tests to obtain managerial insights. We focus on Midtown and Lower Manhattan, a traffic-intensive area of NYC, and divide this area into $|\mathcal{Z}| = 5$ service regions, as shown in Figure 4. Based on the collected data, the average trip duration from one region to a neighboring one is approximately 10 minutes. We set each period as 10 minutes, leading to $T = 144$ periods per day. Table 1 introduces the trip duration $\ell_{z,z'}$ in number of periods between any two service regions $z, z' \in \mathcal{Z}$, $z \neq z'$.

Figure 5 shows the average number of trips over the service regions throughout a day. It is observed that trip demands remain high for the majority of the day, except around 5:00 when they reach their lowest point. Figure 6 shows the average number of trips over the entire operational horizon across the service regions. We set the upper bound $\overline{X}$=4,000 on the total number of EVs

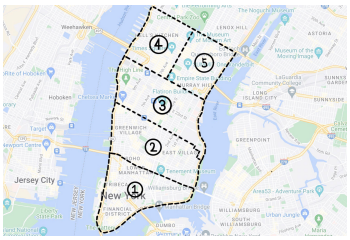

Figure 4 **Service Regions in NYC**

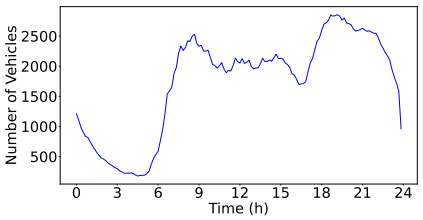

Figure 5 **Average Trips Throughout A Day**

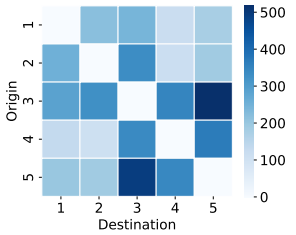

Figure 6 **Average Trips Across Regions**

Table 1 **Trip Duration Across Regions**

Regions	1	2	3	4	5
1	—	1	1	2	2
2	1	—	1	2	2
3	1	1	—	1	1
4	2	2	1	—	1
5	2	2	1	1	—

Table 2 **SoC Usage Across Regions**

Regions	1	2	3	4	5
1	—	1	1	2	2
2	1	—	1	2	2
3	1	1	—	1	1
4	2	2	1	—	1
5	2	2	1	1	—

allocated to all regions[2]. In each region $z \in \mathcal{Z}$, the number X_z^{N} of parking spots without charging or discharging facilities, the number X_z^{C} of parking spots with charging facilities, and the number X_z^{E} of parking spots with bi-directional charging facilities are set as 800, 320, and 160, respectively[3].

Each EV has a battery capacity of 40 kWh, allowing it to run for 6.5 hours or equivalently 38 periods[4]. We assume that each vehicle consumes 1 SoC unit per period while it travels, leading to a maximum electricity consumption of 38 SoC units. Under this assumption, the SoC usage $b_{z,z'}$ to travel between any two regions $z, z' \in \mathcal{Z}$ equals the corresponding trip duration $\ell_{z,z'}$ as shown in Tables 1 and 2. We set the charging rate $\delta^{\mathrm{C}} = 19$ units per period and the discharging rate $\delta^{\mathrm{E}} = 2$ units per period[5]. We estimate the cost parameters in USD. The revenue per EV per period is $c_{\mathrm{R}} = 2.3$, the penalty cost for an unsatisfied trip demand is $c_{\mathrm{P}} = 3c_{\mathrm{R}}$, the relocation cost per EV per period is $c_{\mathrm{L}} = 1.6$, the idle cost per EV per period is $c_{\mathrm{I}} = 0.06$, the battery degradation cost per SoC unit[6] is $c_{\mathrm{deg}} = 0.05$. We assume $P_t^{\mathrm{C}} = P_t^{\mathrm{E}}$ for $t \in \mathcal{T}$. We collect the electricity price for Kansas Central from Evergy (2022) and set $P_t^{\mathrm{C}}(P_t^{\mathrm{E}})$ as follows. We divide each day into four time intervals: super off-peak interval (0:00–6:00), off-peak intervals (6:00–14:00 and 20:00–24:00), and peak interval (14:00–20:00). We set P_t^{C} as 0.1/kWh for $t \in \{1, \ldots, 36\}$ (i.e., 0:00–6:00), 0.15/kWh for $t \in \{37, \ldots, 84\} \cup \{121, \ldots, 144\}$ (i.e., 6:00–14:00 and 20:00–24:00), and 0.27/kWh for $t \in \{85, \ldots, 120\}$ (i.e., 14:00–20:00). The EV allocation cost[7] in any region $z \in \mathcal{Z}$ for SoC $s \in \mathcal{S}$ is $c_s = 72 + 0.15s$.

7.2. Comparing with Other Optimization Approaches

We compare the proposed DRO model ($\mathcal{P}_{\mathrm{F}}$) against models employing sample average approximation (SAA) and robust optimization (RO). Using the SAA approach (Shapiro et al. 2021), given samples $\hat{\boldsymbol{\xi}}_1, \ldots, \hat{\boldsymbol{\xi}}_N$, ($\mathcal{P}_1$) can be approximated as follows:

$$\min_{\mathbf{x}} \left\{ \sum_{z\in\mathcal{Z}} \sum_{s\in\mathcal{S}} c_s x_{z,s} + \sum_{n=1}^{N} \frac{1}{N} f\left(\mathbf{x}, \hat{\boldsymbol{\xi}}_n\right) \middle| (1)-(2) \right\}. \tag{SAA}$$

SAA is widely known to be computationally expensive, especially for a large-scale problem. In our numerical experiments, due to the large-scale nature of the network, we can only solve an SAA model with $N = 3$ scenarios within 24 hours. To ensure that the $N = 3$ scenarios are adequately representative, we utilize a K-means algorithm to cluster all trip-demand samples into three groups based on the magnitude of each sample $\hat{\boldsymbol{\xi}}$ and then select the center of each group (Krishna and Murty 1999). We consider the RO model as a deterministic model under a sample $\hat{\boldsymbol{\xi}}_{\max} \in \{\hat{\boldsymbol{\xi}}_1, \ldots, \hat{\boldsymbol{\xi}}_N\}$, which has the largest magnitude, and formulate it as follows:

$$\min_{\mathbf{x}} \left\{ \sum_{z\in\mathcal{Z}} \sum_{s\in\mathcal{S}} c_s x_{z,s} + f\left(\mathbf{x}, \hat{\boldsymbol{\xi}}_{\max}\right) \middle| (1)-(2) \right\}. \tag{RO}$$

Note that we consider the sample $\hat{\boldsymbol{\xi}}_{\max}$ with the largest magnitude in the RO model because it generally leads to more conservative allocation decisions for the operations. We first solve the proposed DRO, SAA, and RO models based on training data. We use Algorithm 2 to solve the DRO model with $L = 4$, $m = \lfloor 40\% \times |\mathcal{M}| \rfloor$, and $U = 4$. Then, we assess the out-of-sample performance of the allocation solutions under these approaches.

Table 3 Cost Comparison

	Costs ($)		
	Allocation	Operations	Total
DRO	181,080	-304,249	-123,169
SAA	176,976	-296,550	-119,573
RO	209,448	-309,854	-100,405

Table 4 Breakdown of Operations Cost

	Cost ($)						Utilization Rate
	Rental	Penalty	Charging	Discharging	Relocation	Idle	
DRO	-360,451	3,727.6	36,348.1	-802.9	15,100.3	1,828.8	34.9
SAA	-358,933	8,281.1	36,706.1	-656.3	16,575.2	1,477.3	35.6
RO	-361,549	432.5	35,116.9	-767.3	14,148.2	2,765.0	30.4

Table 3 compares the out-of-sample costs of different approaches. It presents the allocation cost (i.e., the cost of allocating vehicles), the operations cost (the cost generated in the second stage), and the total cost (i.e., the sum of allocation and operations costs). It is evident that DRO has the best out-of-sample performance as it generates the lowest total cost. Note that SAA only considers the given samples, which contain limited information of trip-demand correlations, while RO only considers the worst-case scenario, which includes no correlation information. In contrast, by appropriately incorporating correlation information, DRO demonstrates the best performance.

Table 4 provides the breakdown of the operations cost of each approach. Note that we include the rental and discharging revenues as negative costs. Despite incurring a higher allocation cost than SAA, DRO uses a larger fleet to increase revenue from vehicle rentals and discharging and reduces penalty, charging, and relocation costs, leading to a lower total cost. Compared to RO, which has the largest allocation, DRO still achieves a comparable revenue from vehicle rentals because it ensures a higher average utilization rate

$\frac{1}{N'}\sum_{n=1}^{N'}\left(\sum_{(z,t,z')\in\mathcal{M}}\sum_{a\in\hat{\mathcal{A}}^{\mathrm{R}}(z,t,z')} w_a(\hat{\boldsymbol{\xi}}_n)\,/\,\sum_{z\in\mathcal{Z}}\sum_{s\in\mathcal{S}} x_{z,s}\right)$ for each EV, where N' denotes the number of test samples. An operationally efficient system should realize a high average utilization rate for each EV, implying frequent vehicle usage and low idle time during operations. Thus, DRO incurs higher charging and relocation costs but a lower idle cost than RO, as shown in Table 4.

7.3. Comparing Different Correlation Cases

In this section, we investigate the impact of assuming different correlation cases to the DRO approach's performance. We consider three different correlation cases in our problem formulation: (i) **Original Case (benchmark):** We solve Problem ($\mathcal{P}_{\mathrm{M}}$) with $\boldsymbol{\Sigma}$ estimated from the data described in Section 7.1. (ii) **All Case:** We solve Problem (14) by ignoring the covariance constraints. This model allows all possible correlations. (iii) **Independent Case:** We solve Problem ($\mathcal{P}_{\mathrm{M}}$) with $\boldsymbol{\Sigma}^{\mathrm{d}}$, which is a diagonal matrix satisfying $\boldsymbol{\Sigma}^{\mathrm{d}}_{i,i} = \boldsymbol{\Sigma}_{i,i}$ for $i \in \{1,\ldots,|\mathcal{M}|\}$. This model assumes zero covariance between any trip demands, approximating the situation with independent demands. Define

$$\Delta = \frac{\text{Cost of } Y - \text{Cost of Original Case}}{|\text{Cost of Original Case}|} \times 100\%,$$

where Y represents the All Case or Independent Case. Table 5 presents the costs of modeling each correlation case. Obviously, the All Case results in the highest allocation cost with a conservative solution, whereas the Independent Case leads to the lowest allocation cost with an optimistic solution (echoing Propositions 4 and 5, which identify an upper bound and a lower bound, respectively, on the optimal objective value). Since the All Case allows all possible correlations by ignoring the covariance constraints, it results in a conservative solution with a high allocation cost. In contrast, the Independent Case assumes independent trip demands and yields the lowest allocation cost among all the cases. Table 5 shows that the All Case and Independent Case generate a higher total cost than the Original Case, indicating the importance of properly incorporating correlation information into our model to reduce the total cost.

Table 5 Impact of Different Correlation Cases

Cases	Allocation Cost		Operations Cost		Total Cost	
	Val ($)	Δ (%)	Val ($)	Δ (%)	Val ($)	Δ (%)
Original	181,080	0	-304,249	0	-123,169	0
All	189,072	4.41	-307,050	-0.92	-117,978	4.21
Independent	176,184	-2.70	-293,615	3.50	-117,431	4.66

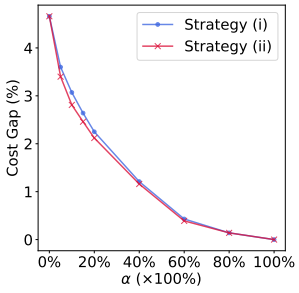

Figure 7 Cost Gap of Considering α-Partial Correlations

7.4. Prioritizing Trip-demand Correlations

The All Case, which allows all possible correlations, and the Independent Case, which assumes no correlations, represent two extreme cases that perform worse than the Original Case. Note that the Original Case considers an ambiguity set confined by the covariance matrix $\mathbf{\Sigma}$. Due to limited resources of the operator, it can be hard to obtain all the entries of $\mathbf{\Sigma}$ in practice. Instead, the operator can consider only correlations between selected trip-demand pairs, while assuming no correlations between other pairs. This may avoid the conservative solution under the All Case and the optimistic solution under the Independent Case. Recall that Section 5.2 introduces two strategies to prioritize the trip-demand pairs: (i) focusing on the pairs with the highest covariance values, and (ii) focusing on the pairs with the largest shadow prices of the covariance constraints (see Proposition 6). We compare these two strategies below.

We first investigate the performance of strategy (i). To do so, we construct a new covariance matrix $\mathbf{\Sigma}^{\mathrm{p}}$ by initializing it with the diagonal covariance matrix, i.e., $\mathbf{\Sigma}^{\mathrm{p}}=\mathbf{\Sigma}^{\mathrm{d}}$. We then incrementally populate the off-diagonal entries of the matrix $\mathbf{\Sigma}^{\mathrm{p}}$ as follows. We first rank the off-diagonal entries $\mathbf{\Sigma}_{i,j}, i \neq j$, of the *original* covariance matrix according to their absolute value from highest to lowest. Thus, we obtain an ordered sequence of indices, $(i_r, j_r), r = 1, \ldots, |\mathcal{M}|^2 - |\mathcal{M}|$, satisfying $|\mathbf{\Sigma}_{i_r,j_r}| \geq |\mathbf{\Sigma}_{i_s,j_s}|$ for $r \leq s$. Given $\alpha \in [0,1]$, let $\mathcal{R}_\Sigma(\alpha) = \{(i_r, j_r), r = 1, \ldots, \lfloor \alpha \times (|\mathcal{M}|^2 - |\mathcal{M}|) \rfloor\}$ be a set of indices of the first α fraction of trip-demand pairs. We set $\mathbf{\Sigma}^{\mathrm{p}}_{i,j} = \mathbf{\Sigma}_{i,j}$, for $(i,j) \in \mathcal{R}_\Sigma(\alpha)$. When α equals 0 and 1, $\mathbf{\Sigma}^{\mathrm{p}}$ corresponds to the Independent Case ($\mathbf{\Sigma}^{\mathrm{p}}=\mathbf{\Sigma}^{\mathrm{d}}$) and the Original Case ($\mathbf{\Sigma}^{\mathrm{p}}=\mathbf{\Sigma}$), respectively. Define the cost gap of the case with $\mathbf{\Sigma}^{\mathrm{p}}$ as follows:

$$\text{Cost Gap} = \frac{\text{Cost of the case with } \mathbf{\Sigma}^{\mathrm{p}} \ - \text{Cost of the Original Case}}{|\text{Cost of the Original Case}|} \times 100\%.$$

We assess the cost gap of including only the α fraction of the off-diagonal entries of $\mathbf{\Sigma}$ (i.e., the cost gap of considering α-partial correlations). Figure 7 shows the cost gap for various α values. It is clear that as we include more covariances of trip-demand pairs (α increases), the cost gap decreases. However, there is diminishing return as more covariances are added. In particular, including the top 40% of covariances of $\mathbf{\Sigma}$ reduces the cost gap from 4.66% to about 1%, while eliminating the remaining 1% gap requires the inclusion of all the covariances. Thus, it is not necessary to estimate all the trip-demand pairs' correlations. Our results serve as a guidance for prioritizing the trip-demand pairs so that a high-quality solution can be obtained.

Next, we assess the performance of strategy (ii). Similar to strategy (i), we first set $\mathbf{\Sigma}^{\mathrm{p}}=\mathbf{\Sigma}^{\mathrm{d}}$. We solve Problem ($\mathcal{P}_{\mathrm{M}}$) using $\mathbf{\Sigma}$ and then obtain the shadow prices $\mathbf{Q}^*$ of the covariance constraints. We rank $Q^*_{i,j}, i,j \in \{1, \ldots, |\mathcal{M}|\}, i \neq j$ from highest to lowest. Define a set $\mathcal{R}_Q(\alpha) = \{(i_r, j_r), r = 1, \ldots, \lfloor \alpha \times (|\mathcal{M}|^2 - |\mathcal{M}|) \rfloor\}$, satisfying $|Q^*_{i_r,j_r}| \geq |Q^*_{i_s,j_s}|$ for $r \leq s$, $\alpha \in [0,1]$. Then, we set $\mathbf{\Sigma}^{\mathrm{p}}_{i,j} = \mathbf{\Sigma}_{i,j}$, for $(i,j) \in \mathcal{R}_Q(\alpha)$. Figure 7 suggests that strategies (i) and (ii) perform similarly, with the cost gap

decreasing as more covariances are included. Strategy (ii) slightly outperforms strategy (i) when α is small because, unlike strategy (i) that only considers covariance values, strategy (ii) also takes the entire optimization problem into account by considering its shadow prices. Strategy (ii) can identify the trip-demand pairs with larger impact on the problem, leading to a smaller cost gap.

7.5. Temporal and Spatial Features of Relocation

We now examine the temporal and spatial features of relocation. Figure 8 shows the number of EVs relocated compared to the total trip demand over the operational horizon. Clearly, relocation occurs throughout the day, with a spike in the periods of rising trip demands. Specifically, relocation peaks occur during 5:00–9:00 and another peak is observed during 17:00–21:00. Both intervals experience significantly rising trip demands. In contrast, when trip demands decrease (e.g., 0:00–5:00 and 21:00–24:00) or remain high (e.g., 9:00–17:00), there is only limited EV relocation. As trip demands increase, more EVs are required in some regions. This necessitates relocating EVs from other regions. Conversely, during periods of decreasing trip demands, fewer EVs are required to be relocated. Similarly, when trip demands are consistently high, the need for relocating EVs is low because many EVs are already distributed across the regions by customers.

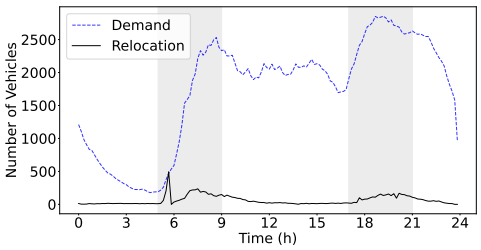

Figure 8 Relocation in A Day

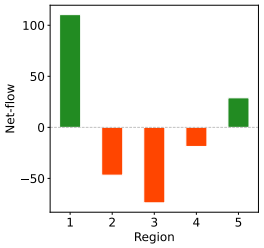

Figure 9 Net-flow of Regions

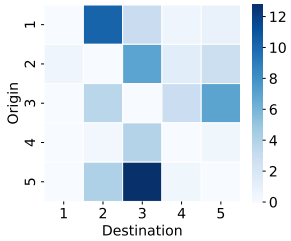

Figure 10 Relocation Across Regions

The above results confirm that relocation is conducted to balance vehicle supply and trip demand during operations. To measure the balance level of each region, define the *net-flow* of each region as the number of trips (equivalently, the number of EVs) entering the region minus the number of trips leaving it. Intuitively, a zero net-flow indicates a balance between EV supply and trip demand, while a positive net-flow reflects an oversupply and a negative net-flow means a shortage. Figure 9 shows the net-flow of each region averaged over the operational horizon. Clearly, Regions 1 and 5 have a positive net-flow, suggesting that these regions gain EVs and may have an oversupply. Therefore, EVs are relocated from these regions to other regions as illustrated in Figure 10. In contrast, Regions 2, 3, and 4 have a negative net-flow, indicating more customers leaving them than entering them. This implies that they lose EVs and may face shortages. Consequently, EVs are relocated to these regions from the others as depicted in Figure 10.

7.6. The Operator's Charging and Discharging Behaviors

A unique feature of the integrated EV allocation and operations problem is the charging and discharging of EVs. In this section, we examine the operator's charging and discharging behaviors over the operational horizon. Figure 11 shows the total electricity charging amount and the charging price over the operational horizon. Clearly, a large number of EVs finish charging during the early hours (0:00–3:00) and are not charged afterward. This is because, during the early hours, both the charging price and the total trip demand (see Figure 5) are low. Therefore, it is cost-effective to charge EVs during these early hours without affecting trip demand fulfillment. Subsequently, both the price and trip demand rise, resulting in a larger number of EVs serving the trip demand, leading to a limited total charging amount. However, we can still observe some EVs that are charged before the price increases (around 6:00 and 14:00) and after the price drops (around 20:00).

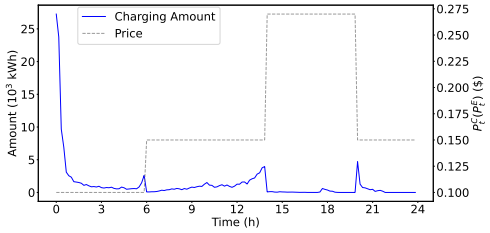

Figure 11 Charging in A Day

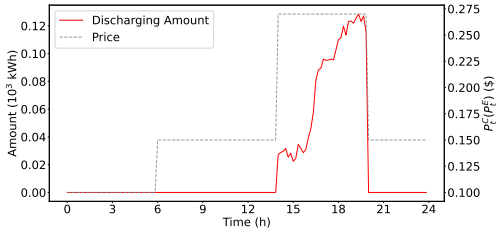

Figure 12 Discharging in A Day

Figure 12 shows the total electricity discharging amount and the discharging price over the operational horizon. It is evident that EVs only discharge electricity to the grid when the discharging price is at its peak. Specifically, more EVs discharge in the later periods of the peak to minimize their risk of electricity shortages that could impact trip demand fulfillment.

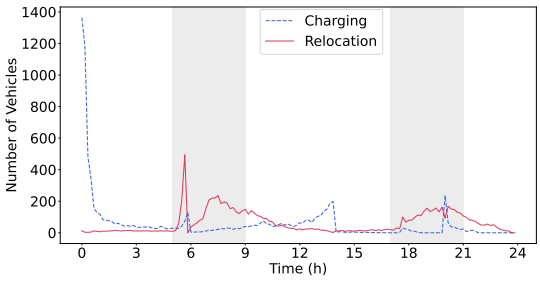

Figure 13 Peaks of EV Relocation Avoid Coinciding with Peaks of EV Charging

Sections 7.5 and 7.6 have examined the relocation and charging of EVs, respectively, over the operational horizon. We now investigate the interaction between EV relocation and charging. Note that when the EVs are being charged in a period, they cannot be relocated to another region at the same time. Figure 13 shows the number of EVs relocated (solid line) and the number of EVs

charged (dashed line) over time. Recall that the peaks of the number of EVs charged are primarily determined by the charging price as shown in Figure 11. Therefore, the peaks of the relocation coincide with the peak hours (5:00–9:00 and 17:00–21:00), but deviate from the peaks of charging as shown in Figure 13. In short, in order to fulfill trip demands, the EV relocation peaks occur when trip demands significantly rise, but avoid coinciding with the peaks of EV charging.

7.7. Impact of Charging Rate

In practice, the charging rate δ^{C} for EVs can be different because of charger technologies. For instance, Tesla offers diverse charging options such as V2 Supercharger stations with a maximum power of 125 kW ($\approx$ 19 SoC/period) and Wall connectors with a maximum power of 11 kW ($\approx$ 2 SoC/period) (Tesla 2024a). In this section, we compare the operator's performance when EVs are charged in a fast mode (δ^{C}=19 SoC/period) and slow mode (δ^{C}=2 SoC/period), while the discharging rate remains as δ^{E}=2 SoC/period.

Table 6 Comparison of Performance in Cases of Different Charging Speeds

Charging Rate (SoC/period)	$\sum_{z,s} x_{z,s}$	Allocation Cost ($)	Operation Cost ($)						Total Cost ($)	Utilization Rate
			Rental	Penalty	Charging	Discharging	Relocation	Idle		
19 (Fast)	2,515	181,080	-360,451	3,727.6	36,348.1	-802.9	15,100.3	1,828.8	-123,169	34.9
2 (Slow)	2,783	200,376	-361,366	982.2	36,813.3	-1,493.8	14,405.4	2,754.4	-107,529	31.8

Table 6 shows that fewer EVs are allocated in the fast-charging mode. Given fewer EVs, higher penalty and relocation costs incur under the fast-charging mode. However, the fast-charging mode generates almost the same rental revenue as the slow-charging mode, with lower charging and idle costs. This can be attributed to the shorter charging times and higher utilization rate of EVs. Overall, the operator incurs a lower total cost under the fast-charging mode.

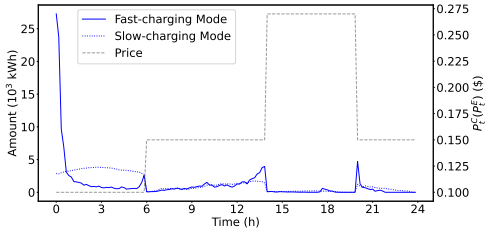

Figure 14 Charging Amount in Different Charging Modes

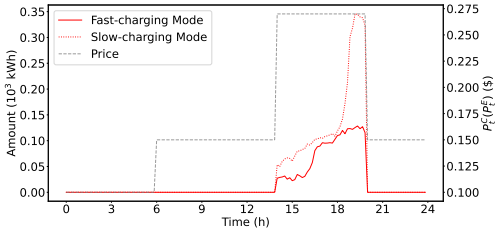

Figure 15 Discharging Amount in Different Charging Modes

Figure 14 shows the total electricity charging amount and the charging price over the operational horizon under both the fast- and slow-charging modes. It suggests that when the charging price is low, the total charging amount remains consistently high under the slow mode (dotted line). This is very different from the behavior under the fast-charging mode (solid line), where the charging process is obviously shorter and its peak value reaches a significantly higher level

($\approx 25\times10^3$kWh). This discrepancy exists because the slow-charging mode requires more time to attain the same SoC compared to the fast-charging mode. Figure 15 shows that similar to fast charging, under the slow-charging mode, EVs only discharge when the discharging price is peaked, and most EVs discharge in the later periods during the peak. The peak value under the slow-charging mode (dotted line) is substantially higher because there are more EVs allocated under this mode and they discharge at the same time right before the discharging price drops.

7.8. Impact of Pricing Scheme for Charging

In practice, there are different pricing schemes for charging EVs, including those based on charging amount (in kWh) and those based on charging time (in minutes) (Tesla 2024b). Recall that all the numerical experiments above use the pricing scheme based on charging amount (see Section 3.3). We now investigate the operator's performance under the pricing scheme based on charging time. Since the charging rate is δ^{C} and the unit charging price in period t is P_t^{C}, the electricity charging price per period is $P_t^{\mathrm{Time}} = \delta^{\mathrm{C}} P_t^{\mathrm{C}}$ in period t. For charging arc $a = (n_{z,t,s}, n_{z,t+1,s'}) \in \mathcal{A}^{\mathrm{C}}$, we set $c_a = P_t^{\mathrm{Time}} + c_{\mathrm{deg}}$. Note that the pricing scheme for discharging remains unchanged (i.e., based on discharging amount described in Section 3.3).

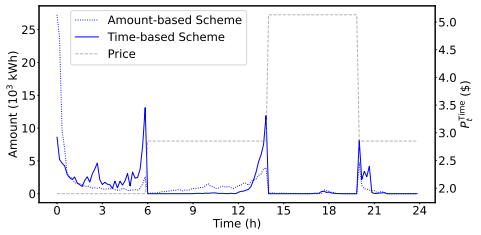

Figure 16 Charging in A Day Under Time-based Pricing Scheme

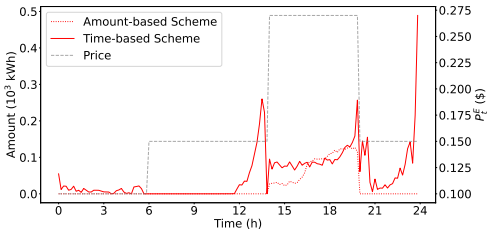

Figure 17 Discharging in A Day Under Time-based Pricing Scheme

Under the time-based pricing scheme, the operator pays P_t^{Time} in period t regardless of the actual charging amount. This may lead to different charging and discharging behaviors compared to that under the amount-based pricing scheme in Figures 11 and 12. Figure 16 shows the total electricity charging amount (solid line) over the operational horizon under the time-based pricing scheme. We observe two notable peaks during the early hours (0:00–6:00) when the charging price is low. Specifically, one peak occurs around 0:00, while the other occurs right before 6:00. This charging behavior is different from that under the amount-based pricing scheme (dotted line), where only one peak with a much higher value occurs around 0:00. This is because under the time-based pricing scheme, a fixed cost P_t^{Time} is paid per period regardless of the charging amount. Since the charging rate is δ^{C}=19 SoC/period, it will be disadvantageous to the operator if the charging amount is less than 19 SoC per period. Thus, some EVs do not charge initially until their SoC drops to a low level, leading to a smaller total charging amount around 0:00 and a larger total charging amount right before 6:00 compared to the amount-based pricing scheme.

In addition, Figure 16 shows that the total charging amount before the price rises (around 14:00) and after the price drops (around 20:00) are obviously higher than that under the amount-based pricing scheme. Interestingly, Figure 17 shows that the total discharging amount surges immediately before each of these charging peaks. This is because discharging before charging its EVs allows the operator to earn additional revenue as it pays a fixed cost P_t^{Time} per period for charging. Furthermore, EVs are charged with excess electricity under the time-based pricing scheme. Thus, a large discharging amount occurs at the end of the day as shown in Figure 17.

8. Conclusion

Managing a shared mobility system with EVs equipped with V2G technology is especially challenging because of their time-consuming charging and discharging. The operator of such a system needs to carefully plan the initial vehicle allocation for different service regions. To do so, it is crucial for the operator to take the future operations into consideration. This requires a model that integrates initial EV allocation decisions and subsequent operations decisions. The uncertain nature of trip demands significantly increases the complexity of the problem. Furthermore, it is important to consider the correlations between trip demands across service regions and time periods. Due to the operator's limited resources, it is impractical to obtain perfect knowledge of these correlations. Fortunately, we can adopt DRO to effectively capture correlated trip-demand uncertainties without requiring the perfect knowledge of the correlations.

We formulate the integrated EV allocation and operations problem with correlated demand uncertainties as a two-stage DRO problem ($\mathcal{P}_{\text{M}}$) on a time-space-SoC network (see Figure 3). The operator's objective is to minimize its expected cost under a worst-case joint distribution within an ambiguity set, which is constructed based on the support, first-, and second-moment information of uncertain demands. In the first stage, the operator decides the initial EV allocation before trip demands are realized. In the second stage where correlated demands are observed, the operator manages EVs across regions to meet the trip demands over multiple periods.

We reformulate the two-stage DRO problem ($\mathcal{P}_{\text{M}}$) as an SDP problem ($\mathcal{P}_{\text{F}}$) (see Theorem 1 and Propositions 1–2). The covariance matrix $\mathbf{\Sigma}$ of demand uncertainties, characterizing the correlation information, plays a critical role in solving the problem. We show that the optimal cost of ($\mathcal{P}_{\text{M}}$) is monotonic in $\mathbf{\Sigma}$ (see Proposition 3). We also identify upper and lower bounds on the optimal total cost (see Propositions 4 and 5). Furthermore, we assess the impact of the correlation of each trip-demand pair by calculating the shadow prices of covariance constraints (see Proposition 6). Using these shadow prices, the operator can prioritize trip-demand pairs. To overcome the computational difficulty of solving the SDP problem ($\mathcal{P}_{\text{F}}$), we introduce three approximation approaches: (i) outer approximation that provides a lower bound on the optimal objective value

(see Theorem 2 and Proposition 7), (ii) inner approximation that provides an upper bound (see Theorem 3 and Proposition 8), and (iii) Algorithm 1 that considers only a portion of $vert(\mathcal{Y})$. Based on these approximation approaches, we develop Algorithm 2 that decomposes network $\mathcal{G}$ into sub-networks and solves each one sequentially.

Our numerical experiments using real data from TLC in NYC suggest that the proposed DRO approach outperforms SAA and RO in terms of out-of-sample cost (see Section 7.2). We further investigate the impact of assuming different correlation cases to DRO's performance, highlighting the value of properly incorporating correlation information, which attains up to 4.66% total cost reduction (see Section 7.3). However, due to the operator's limited resources, it can be hard to incorporate complete correlation information in practice. In this situation, the operator can prioritize the trip-demand pairs based on two strategies: (i) focusing on the pairs with the highest covariance values and (ii) focusing on the pairs with the largest shadow prices of the covariance constraints. Strategy (ii) slightly outperforms strategy (i). Both result in a lower cost as more covariances are included (see Section 7.4).

Our out-of-sample experiment results reveal that relocation peaks when demands significantly rise, and EVs are relocated from regions with an oversupply to regions with shortages (see Section 7.5). Most EVs finish charging during early hours when the charging price and the total trip demand are low, and some EVs charge before the price increases and after the price drops. Most EVs discharge when the discharging price is high. We also note that the peaks of relocation deviate from the peaks of charging (see Section 7.6). A larger charging rate leads to a reduction in EV allocation and a drop in total cost (see Section 7.7). Finally, a time-based pricing scheme for charging EVs leads to more charging peaks and a larger total discharging amount compared to an amount-based pricing scheme (see Section 7.8).

We believe that our approaches can effectively address other OM/OR problems that involve correlated uncertainties, such as power system operations where renewable energy generation is correlated, and supply chain management where supply risks are correlated. Additionally, exploring alternative ambiguity sets could be beneficial. For example, we may consider using a discrepancy-based ambiguity set based on the Wasserstein metric (Esfahani and Kuhn 2017). We leave these for future research.

References

Ai, W., Deng, T., and Qi, W. (2021). Crowdsourcing electric mobility for omni-sharing distributed energy resources. *Available at SSRN 3984370*.

Alismail, F., Xiong, P., and Singh, C. (2017). Optimal wind farm allocation in multi-area power systems using distributionally robust optimization approach. *IEEE Transactions on Power Systems*, 33(1):536–544.

Basciftci, B., Ahmed, S., and Shen, S. (2021). Distributionally robust facility location problem under decision-dependent stochastic demand. *European Journal of Operational Research*, 292(2):548–561.

Benjaafar, S. and Hu, M. (2020). Operations management in the age of the sharing economy: What is old and what is new? *Manufacturing & Service Operations Management*, 22(1):93–101.

Benjaafar, S., Wu, S., Liu, H., and Gunnarsson, E. B. (2022). Dimensioning on-demand vehicle sharing systems. *Management Science*, 68(2):1218–1232.

Chen, Q., Lei, Y., and Jasin, S. (2024). Real-time spatial–intertemporal pricing and relocation in a ride-hailing network: Near-optimal policies and the value of dynamic pricing. *Operations Research*, 72(5):2097–2118.

Cheramin, M., Cheng, J., Jiang, R., and Pan, K. (2022). Computationally efficient approximations for distributionally robust optimization under moment and Wasserstein ambiguity. *INFORMS Journal on Computing*, 34(3):1768–1794.

Cui, Z., Long, D. Z., Qi, J., and Zhang, L. (2023). The inventory routing problem under uncertainty. *Operations Research*, 71(1):378–395.

Delage, E. and Ye, Y. (2010). Distributionally robust optimization under moment uncertainty with application to data-driven problems. *Operations Research*, 58(3):595–612.

Dong, Y., De Koster, R., Roy, D., and Yu, Y. (2022). Dynamic vehicle allocation policies for shared autonomous electric fleets. *Transportation Science*, 56(5):1238–1258.

E.ON (2024). *Electric car battery capacity & lifespan*. Accessed: January 4, 2024.

Esfahani, P. M. and Kuhn, D. (2017). Data-driven distributionally robust optimization using the Wasserstein metric: Performance guarantees and tractable reformulations. *Mathematical Programming*, 171(1-2):115–166.

Evergy (2022). *Business EV Rate Plan*. Accessed: January 4, 2024.

Fathabad, A. M., Cheng, J., Pan, K., and Qiu, F. (2020). Data-driven planning for renewable distributed generation integration. *IEEE Transactions on Power Systems*, 35(6):4357–4368.

Gao, R. (2023). Finite-sample guarantees for Wasserstein distributionally robust optimization: Breaking the curse of dimensionality. *Operations Research*, 71(6):2291–2306.

Ghosal, S. and Wiesemann, W. (2020). The distributionally robust chance-constrained vehicle routing problem. *Operations Research*, 68(3):716–732.

Goh, J. and Sim, M. (2010). Distributionally robust optimization and its tractable approximations. *Operations Research*, 58(4-part-1):902–917.

Grasen (2021). *The largest V2G project for vehicle network interaction in industrial parks in China is officially put into operation*. Accessed: January 4, 2024.

He, L., Hu, Z., and Zhang, M. (2020). Robust repositioning for vehicle sharing. *Manufacturing & Service Operations Management*, 22(2):241–256.

He, L., Ma, G., Qi, W., and Wang, X. (2021a). Charging an electric vehicle-sharing fleet. *Manufacturing & Service Operations Management*, 23(2):471–487.

He, L., Mak, H.-Y., Rong, Y., and Shen, Z.-J. M. (2017). Service region design for urban electric vehicle sharing systems. *Manufacturing & Service Operations Management*, 19(2):309–327.

He, P., Zheng, F., Belavina, E., and Girotra, K. (2021b). Customer preference and station network in the london bike-share system. *Management Science*, 67(3):1392–1412.

Jiang, S., Cheng, J., Pan, K., and Shen, Z.-J. M. (2023). Optimized dimensionality reduction for moment-based distributionally robust optimization. *arXiv preprint arXiv:2305.03996*.

Jin, Z., Wang, Y., Lim, Y. F., Pan, K., and Shen, Z.-J. M. (2023). Vehicle rebalancing in a shared micromobility system with rider crowdsourcing. *Manufacturing & Service Operations Management*, 25(4):1394–1415.

Krishna, K. and Murty, M. N. (1999). Genetic k-means algorithm. *IEEE Transactions on Systems, Man, and Cybernetics, Part B (Cybernetics)*, 29(3):433–439.

Lauinger, D., Vuille, F., and Kuhn, D. (2024). Reliable frequency regulation through vehicle-to-grid: Encoding legislation with robust constraints. *Manufacturing & Service Operations Management*, 26(2):722–738.

Li, H., Delage, E., Zhu, N., Pinedo, M., and Ma, S. (2024). Distributional robustness and inequity mitigation in disaster preparedness of humanitarian operations. *Manufacturing & Service Operations Management*, 26(1):197–214.

Liu, J., Sun, L., Chen, W., and Xiong, H. (2016). Rebalancing bike sharing systems: A multi-source data smart optimization. In *Proceedings of the 22nd ACM SIGKDD International Conference on Knowledge Discovery and Data Mining*, pages 1005–1014.

Lu, M., Chen, Z., and Shen, S. (2018). Optimizing the profitability and quality of service in carshare systems under demand uncertainty. *Manufacturing & Service Operations Management*, 20(2):162–180.

Nair, R. and Miller-Hooks, E. (2011). Fleet management for vehicle sharing operations. *Transportation Science*, 45(4):524–540.

Nasdaq (2022). *PG&E to Offer Nation's First Vehicle-To-Grid Export Rate for Commercial Electric Vehicles*. Accessed: January 4, 2024.

NYC DOT (2021). *An Electric Vehicle Vision Plan for New York City*. Accessed: January 4, 2024.

NYC DOT (2024). *25 mph Speed Limit*. Accessed: January 4, 2024.

Qi, W., Li, L., Liu, S., and Shen, Z.-J. M. (2018). Shared mobility for last-mile delivery: Design, operational prescriptions, and environmental impact. *Manufacturing & Service Operations Management*, 20(4):737–751.

Qi, W., Sha, M., and Li, S. (2022). When shared autonomous electric vehicles meet microgrids: Citywide energy-mobility orchestration. *Manufacturing & Service Operations Management*, 24(5):2389–2406.

Rahimian, H. and Mehrotra, S. (2019). Distributionally robust optimization: A review. *arXiv preprint arXiv:1908.05659*.

Scarf, H. (1958). A min-max solution of an inventory problem. *Studies in the Mathematical Theory of Inventory and Production*.

Shapiro, A. (2001). On duality theory of conic linear problems. *Nonconvex Optimization and its Applications*, 57:135–155.

Shapiro, A., Dentcheva, D., and Ruszczynski, A. (2021). *Lectures on Stochastic Programming: Modeling and Theory*. SIAM.

Shu, J., Chou, M. C., Liu, Q., Teo, C.-P., and Wang, I.-L. (2013). Models for effective deployment and redistribution of bicycles within public bicycle-sharing systems. *Operations Research*, 61(6):1346–1359.

Soppert, M., Steinhardt, C., Müller, C., and Gönsch, J. (2022). Differentiated pricing of shared mobility systems considering network effects. *Transportation Science*, 56(5):1279–1303.

Tesla (2024a). *Wall Connector*. Accessed: January 4, 2024.

Tesla (2024b). *Supercharger Support*. Accessed: January 4, 2024.

The New York Times (2023). *Electric Vehicles Could Match Gasoline Cars on Price This Year*. Accessed: January 4, 2024.

TLC (2024). *TLC Trip Record Data*. Accessed: January 4, 2024.

Uber (2023). *Our Road to Zero Emissions*. Accessed: January 4, 2024.

UC Riverside (2024). *Zipcar provides wheels when you want them*. Accessed: January 4, 2024.

Vazirani, V. V. (2001). *Approximation algorithms*, volume 1. Springer.

Widrick, R. S., Nurre, S. G., and Robbins, M. J. (2018). Optimal policies for the management of an electric vehicle battery swap station. *Transportation Science*, 52(1):59–79.

Wiesemann, W., Kuhn, D., and Sim, M. (2014). Distributionally robust convex optimization. *Operations Research*, 62(6):1358–1376.

Xin, L. and Goldberg, D. A. (2022). Distributionally robust inventory control when demand is a martingale. *Mathematics of Operations Research*, 47(3):2387–2414.

Zapmap (2020). *Nissan and E.On V2G charging project to expand*. Accessed: January 4, 2024.

Zhang, R. and Kincaid, R. (2014). Robust optimization model for runway configurations management. *International Journal of Operations Research and Information Systems*, 5(3):1–26.

Zhang, Y., Lu, M., and Shen, S. (2021). On the values of vehicle-to-grid electricity selling in electric vehicle sharing. *Manufacturing & Service Operations Management*, 23(2):488–507.

Zipcar (2024). *Electric car hire with Zipcar*. Accessed: January 4, 2024.

Appendix A: Proof of Theorem 1

This result is deduced from Lemma 1 in Delage and Ye (2010). □

Appendix B: Proof of Proposition 1

We define the following dual multipliers with respect to constraints (3)–(9):

$$\pi^0_{z,s} \in \mathbb{R},\ \forall z \in \mathcal{Z},\ s \in \mathcal{S},$$
$$\pi_{z,t,s} \in \mathbb{R},\ \forall z \in \mathcal{Z},\ t \in \{1,\dots T-1\},\ s \in \mathcal{S},$$
$$\pi^{\mathrm{T}} \in \mathbb{R},$$
$$\omega_{z,t,z'} \le 0,\ \forall (z,t,z') \in \mathcal{M},$$
$$\phi_{z,t} \le 0,\ \forall z \in \mathcal{Z},\ t \in \mathcal{T},$$
$$\phi^{\mathrm{C}}_{z,t} \le 0,\ \forall z \in \mathcal{Z},\ t \in \mathcal{T},$$
$$\phi^{\mathrm{E}}_{z,t} \le 0,\ \forall z \in \mathcal{Z},\ t \in \mathcal{T}.$$

We use $\boldsymbol{\pi}$ to denote the vector of all the above dual variables.

With any given $(\mathbf{x}, \boldsymbol{\xi})$, we can formulate the dual problem of the second-stage problem $(\mathcal{P}_2)$ as

$$\begin{aligned} f'(\mathbf{x},\boldsymbol{\xi}) = \max\ & \sum_{z\in\mathcal{Z}}\sum_{s\in\mathcal{S}} \pi^0_{z,s}x_{z,s} + \pi^{\mathrm{T}} \sum_{z\in\mathcal{Z}}\sum_{s\in\mathcal{S}} x_{z,s} + \sum_{z\in\mathcal{Z}}\sum_{t\in\mathcal{T}} \phi_{z,t} \sum_{k\in\mathcal{K}} X^k_z + \sum_{z\in\mathcal{Z}}\sum_{t\in\mathcal{T}} \phi^{\mathrm{C}}_{z,t}\left(X^{\mathrm{C}}_z + X^{\mathrm{E}}_z\right) \qquad (\mathcal{P}_{\mathrm{d}}) \\ & + \sum_{z\in\mathcal{Z}}\sum_{t\in\mathcal{T}} \phi^{\mathrm{E}}_{z,t}X^{\mathrm{E}}_z + \sum_{(z,t,z')\in\mathcal{M}} d_{z,t,z'}(\boldsymbol{\xi})\omega_{z,t,z'} + c_{\mathrm{P}} \sum_{(z,t,z')\in\mathcal{M}} d_{z,t,z'}(\boldsymbol{\xi}) \\ \text{s.t. } & \pi^0_{z,s} - \pi_{z,1,s} + \phi_{z,0} \le c_{\mathrm{I}},\ \forall (z,0,s) \in \mathcal{W}^{\mathrm{I}}, \qquad (\text{EC.1}) \\ & \pi_{z,t,s} - \pi_{z',t',s'} + \omega_{z,t,z'} \le -c_{\mathrm{R}}\ell_{z,z'} - c_{\mathrm{P}},\ \forall t' \in \{2,\dots,T-1\},\ (z,z',t,t',s,s') \in \mathcal{W}^{\mathrm{R}}, \qquad (\text{EC.2}) \\ & \pi_{z,t,s} - \pi_{z,t+1,s} + \phi_{z,t} \le c_{\mathrm{I}},\ \forall t \in \{1,\dots,T-2\},\ (z,t,s) \in \mathcal{W}^{\mathrm{I}}, \qquad (\text{EC.3}) \\ & \pi_{z,t,s} - \pi_{z',t',s} \le c_{\mathrm{L}}\ell_{z,z'},\ \forall t' \in \{2,\dots,T-1\},\ (z,z',t,t',s) \in \mathcal{W}^{\mathrm{L}}, \qquad (\text{EC.4}) \\ & \pi_{z,t,s} - \pi_{z,t+1,s'} + \phi_{z,t} + \phi^{\mathrm{C}}_{z,t} \le \beta^{\mathrm{C}}_{t,s,s'},\ \forall t \in \{1,\dots,T-2\},\ (z,t,s,s') \in \mathcal{W}^{\mathrm{C}}, \qquad (\text{EC.5}) \\ & \pi_{z,t,s} - \pi_{z,t+1,s'} + \phi_{z,t} + \phi^{\mathrm{C}}_{z,t} + \phi^{\mathrm{E}}_{z,t} \le \beta^{\mathrm{E}}_{t,s,s'},\ \forall t \in \{1,\dots,T-2\},\ (z,t,s,s') \in \mathcal{W}^{\mathrm{E}}, \qquad (\text{EC.6}) \\ & \pi^{\mathrm{T}} + \pi_{z,T-\ell_{z,z'},s} + \omega_{z,T-\ell_{z,z'},z'} \le -c_{\mathrm{R}}\ell_{z,z'} - c_{\mathrm{P}},\ \forall (z,z',T-\ell_{z,z'},T,s,s') \in \mathcal{W}^{\mathrm{R}}, \qquad (\text{EC.7}) \\ & \pi^{\mathrm{T}} + \pi_{z,T-1,s} + \phi_{z,T-1} \le c_{\mathrm{I}},\ \forall (z,T-1,s) \in \mathcal{W}^{\mathrm{I}}, \qquad (\text{EC.8}) \\ & \pi^{\mathrm{T}} + \pi_{z,T-\ell_{z,z'},s} \le c_{\mathrm{L}}\ell_{z,z'},\ \forall (z,z',T-\ell_{z,z'},T,s) \in \mathcal{W}^{\mathrm{L}}, \qquad (\text{EC.9}) \\ & \pi^{\mathrm{T}} + \pi_{z,T-1,s} + \phi_{z,T-1} + \phi^{\mathrm{C}}_{z,T-1} \le \beta^{\mathrm{C}}_{T-1,s,s'},\ \forall (z,T-1,s,s') \in \mathcal{W}^{\mathrm{C}}, \qquad (\text{EC.10}) \\ & \pi^{\mathrm{T}} + \pi_{z,T-1,s} + \phi_{z,T-1} + \phi^{\mathrm{C}}_{z,T-1} + \phi^{\mathrm{E}}_{z,T-1} \le \beta^{\mathrm{E}}_{T-1,s,s'},\ \forall (z,T-1,s,s') \in \mathcal{W}^{\mathrm{E}}, \qquad (\text{EC.11}) \\ & \omega_{z,t,z'} \le 0,\ \forall (z,t,z') \in \mathcal{M};\ \phi_{z,t},\ \phi^{\mathrm{C}}_{z,t},\ \phi^{\mathrm{E}}_{z,t} \le 0,\ \forall z \in \mathcal{Z},\ t \in \mathcal{T}. \qquad (\text{EC.12}) \end{aligned}$$

Thus, we define

$$\begin{aligned} \psi(\mathbf{x},\boldsymbol{\pi},\boldsymbol{\xi}) = & \sum_{z\in\mathcal{Z}}\sum_{s\in\mathcal{S}} \pi^0_{z,s}x_{z,s} + \pi^{\mathrm{T}} \sum_{z\in\mathcal{Z}}\sum_{s\in\mathcal{S}} x_{z,s} + \sum_{z\in\mathcal{Z}}\sum_{t\in\mathcal{T}} \phi_{z,t} \sum_{k\in\mathcal{K}} X^k_z + \sum_{z\in\mathcal{Z}}\sum_{t\in\mathcal{T}} \phi^{\mathrm{C}}_{z,t}\left(X^{\mathrm{C}}_z + X^{\mathrm{E}}_z\right) \\ & + \sum_{z\in\mathcal{Z}}\sum_{t\in\mathcal{T}} \phi^{\mathrm{E}}_{z,t}X^{\mathrm{E}}_z + \sum_{(z,t,z')\in\mathcal{M}} d_{z,t,z'}(\boldsymbol{\xi})\omega_{z,t,z'} + c_{\mathrm{P}} \sum_{(z,t,z')\in\mathcal{M}} d_{z,t,z'}(\boldsymbol{\xi}), \qquad (\text{EC.13}) \end{aligned}$$

and use $\mathcal{Y}$ to denote the feasible region defined by constraints (EC.1)–(EC.12). Then we can write Problem $(\mathcal{P}_{\rm d})$ in the abstract form: $\max_{\boldsymbol{\pi}\in\mathcal{Y}} \psi(\mathbf{x},\boldsymbol{\pi},\boldsymbol{\xi})$.

By the strong duality theorem, we have $f(\mathbf{x},\boldsymbol{\xi}) = f'(\mathbf{x},\boldsymbol{\xi}) = \max_{\boldsymbol{\pi}\in\mathcal{Y}} \psi(\mathbf{x},\boldsymbol{\pi},\boldsymbol{\xi})$, with any given $(\mathbf{x},\boldsymbol{\xi})$. Therefore, we can equivalently rewrite Problem $(\mathcal{P}_{\rm in})$ as

$$\begin{aligned}\min_{\mathbf{Q}\succeq 0,\mathbf{q},r}\ & r + \left(\gamma_2\boldsymbol{\Sigma} + \boldsymbol{\mu}\boldsymbol{\mu}^\top\right)\bullet\mathbf{Q} + \boldsymbol{\mu}^\top\mathbf{q} + \sqrt{\gamma_1}\left\|\boldsymbol{\Sigma}^{\frac{1}{2}}\left(\mathbf{q}+2\mathbf{Q}\boldsymbol{\mu}\right)\right\|_2\\ \text{s.t. }& r \geq \max_{\boldsymbol{\pi}\in\mathcal{Y}} \psi\left(\mathbf{x},\boldsymbol{\pi},\boldsymbol{\xi}\right) - \boldsymbol{\xi}^\top\mathbf{Q}\boldsymbol{\xi} - \boldsymbol{\xi}^\top\mathbf{q},\ \forall\,\boldsymbol{\xi}\in\Omega.\end{aligned}$$

It is well known that the optimal solution of a linear programming problem with a non-empty and compact feasible set is adopted at a vertex (Esfahani and Kuhn 2017). This means $\max_{\boldsymbol{\pi}\in\mathcal{Y}} \psi(\mathbf{x},\boldsymbol{\pi},\boldsymbol{\xi}) = \max_{\boldsymbol{\pi}\in vert(\mathcal{Y})} \psi(\mathbf{x},\boldsymbol{\pi},\boldsymbol{\xi})$. Thus, we have Proposition 1 holds. □

Appendix C: Proof of Proposition 2

Constraints (13) in Problem $(\mathcal{P}'_{\rm in})$ are equivalent to $\min_{\boldsymbol{\xi}\in\Omega}\ g(\boldsymbol{\xi},\boldsymbol{\pi}) \geq 0$ for any $\boldsymbol{\pi}\in vert(\mathcal{Y})$, where $g(\boldsymbol{\xi},\boldsymbol{\pi}) = r - \psi(\mathbf{x},\boldsymbol{\pi},\boldsymbol{\xi}) + \boldsymbol{\xi}^\top\mathbf{Q}\boldsymbol{\xi} + \boldsymbol{\xi}^\top\mathbf{q}$. Given that $\Omega = \{\boldsymbol{\xi}\in\mathbb{R}^{|\mathcal{M}|} \mid \mathbf{b}^{\rm lb} \leq \mathbf{A}\boldsymbol{\xi} \leq \mathbf{b}^{\rm ub}\}$, we consider the Lagrange dual problem of $\min_{\boldsymbol{\xi}\in\Omega}\ g(\boldsymbol{\xi},\boldsymbol{\pi})$, i.e., $\max_{\boldsymbol{\lambda}_1,\boldsymbol{\lambda}_2\geq\mathbf{0}} \min_{\boldsymbol{\xi}\in\mathbb{R}^{|\mathcal{M}|}}\ g(\boldsymbol{\xi},\boldsymbol{\pi}) + \boldsymbol{\lambda}_1^\top(\mathbf{A}\boldsymbol{\xi} - \mathbf{b}^{\rm ub}) - \boldsymbol{\lambda}_2^\top(\mathbf{A}\boldsymbol{\xi} - \mathbf{b}^{\rm lb})$. Note that $g(\boldsymbol{\xi},\boldsymbol{\pi})$ is convex in $\boldsymbol{\xi}$ because $\mathbf{Q}\succeq 0$. It follows that constraints (13) are equivalent to the following ones:

$$\max_{\boldsymbol{\lambda}_1,\boldsymbol{\lambda}_2\geq\mathbf{0}} \min_{\boldsymbol{\xi}\in\mathbb{R}^{|\mathcal{M}|}} g\left(\boldsymbol{\xi},\boldsymbol{\pi}\right) + \boldsymbol{\lambda}_1^\top\left(\mathbf{A}\boldsymbol{\xi} - \mathbf{b}^{\rm ub}\right) - \boldsymbol{\lambda}_2^\top\left(\mathbf{A}\boldsymbol{\xi} - \mathbf{b}^{\rm lb}\right) \geq 0,\ \forall\,\boldsymbol{\pi}\in vert\left(\mathcal{Y}\right),$$

which are further equivalent to the following constraints:

$$\begin{aligned}\exists\boldsymbol{\lambda}_1,\boldsymbol{\lambda}_2\geq\mathbf{0},\ & r - \psi\left(\mathbf{x},\boldsymbol{\pi},\boldsymbol{\xi}\right) + \boldsymbol{\xi}^\top\mathbf{Q}\boldsymbol{\xi} + \boldsymbol{\xi}^\top\mathbf{q} + \boldsymbol{\lambda}_1^\top\left(\mathbf{A}\boldsymbol{\xi} - \mathbf{b}^{\rm ub}\right) - \boldsymbol{\lambda}_2^\top\left(\mathbf{A}\boldsymbol{\xi} - \mathbf{b}^{\rm lb}\right) \geq 0,\\ &\qquad\qquad \forall\,\boldsymbol{\xi}\in\mathbb{R}^{|\mathcal{M}|},\ \boldsymbol{\pi}\in vert\left(\mathcal{Y}\right). \quad \text{(EC.14)}\end{aligned}$$

By definition of $\psi(\mathbf{x},\boldsymbol{\pi},\boldsymbol{\xi})$, i.e., (EC.13), we can rewrite (EC.14) as:

$$\begin{aligned}\exists\boldsymbol{\lambda}_1,\boldsymbol{\lambda}_2\geq\mathbf{0},\ & r - \sum_{z\in\mathcal{Z}}\sum_{s\in\mathcal{S}}\pi^0_{z,s}x_{z,s} - \pi^{\rm T}\sum_{z\in\mathcal{Z}}\sum_{s\in\mathcal{S}}x_{z,s} - \sum_{z\in\mathcal{Z}}\sum_{t\in\mathcal{T}}\phi_{z,t}\sum_{k\in\mathcal{K}}X_z^k - \sum_{z\in\mathcal{Z}}\sum_{t\in\mathcal{T}}\phi^{\rm C}_{z,t}\left(X_z^{\rm C}+X_z^{\rm E}\right) - \sum_{z\in\mathcal{Z}}\sum_{t\in\mathcal{T}}\phi^{\rm E}_{z,t}X_z^{\rm E}\\ &- \boldsymbol{\omega}^\top\boldsymbol{\xi} - \mathbf{c}_{\rm P}^\top\boldsymbol{\xi} + \boldsymbol{\xi}^\top\mathbf{Q}\boldsymbol{\xi} + \mathbf{q}^\top\boldsymbol{\xi}\\ &+ \boldsymbol{\lambda}_1^\top\left(\mathbf{A}\boldsymbol{\xi} - \mathbf{b}^{\rm ub}\right) - \boldsymbol{\lambda}_2^\top\left(\mathbf{A}\boldsymbol{\xi} - \mathbf{b}^{\rm lb}\right) \geq 0,\ \forall\,\boldsymbol{\xi}\in\mathbb{R}^{|\mathcal{M}|},\ \boldsymbol{\pi}\in vert\left(\mathcal{Y}\right),\end{aligned}$$

which are equivalent to

$$\begin{aligned}\exists\boldsymbol{\lambda}_1,\boldsymbol{\lambda}_2\geq\mathbf{0},\ & \boldsymbol{\xi}^\top\mathbf{Q}\boldsymbol{\xi} + r - \psi_1\left(\mathbf{x},\boldsymbol{\pi}\right) - \boldsymbol{\lambda}_1^\top\mathbf{b}^{\rm ub} + \boldsymbol{\lambda}_2^\top\mathbf{b}^{\rm lb} + \left(\mathbf{q} + \mathbf{A}^\top\left(\boldsymbol{\lambda}_1 - \boldsymbol{\lambda}_2\right) - \psi_2\left(\boldsymbol{\pi}\right)\right)^\top\boldsymbol{\xi} \geq 0,\\ &\qquad\qquad \forall\,\boldsymbol{\xi}\in\mathbb{R}^{|\mathcal{M}|},\ \boldsymbol{\pi}\in vert\left(\mathcal{Y}\right), \quad \text{(EC.15)}\end{aligned}$$

where

$$\begin{aligned}&\psi_1\left(\mathbf{x},\boldsymbol{\pi}\right) = \sum_{z\in\mathcal{Z}}\sum_{s\in\mathcal{S}}\pi^0_{z,s}x_{z,s} + \pi^{\rm T}\sum_{z\in\mathcal{Z}}\sum_{s\in\mathcal{S}}x_{z,s} + \sum_{z\in\mathcal{Z}}\sum_{t\in\mathcal{T}}\phi_{z,t}\sum_{k\in\mathcal{K}}X_z^k + \sum_{z\in\mathcal{Z}}\sum_{t\in\mathcal{T}}\phi^{\rm C}_{z,t}\left(X_z^{\rm C}+X_z^{\rm E}\right) + \sum_{z\in\mathcal{Z}}\sum_{t\in\mathcal{T}}\phi^{\rm E}_{z,t}X_z^{\rm E},\\ &\psi_2\left(\boldsymbol{\pi}\right) = \boldsymbol{\omega} + \mathbf{c}_{\rm P}.\end{aligned}$$

Thus, we have

$$\text{(EC.15)} \Leftrightarrow \exists \boldsymbol{\lambda}_1, \boldsymbol{\lambda}_2 \geq \mathbf{0},\ \left(1, \boldsymbol{\xi}^\top\right) \mathbf{V} \left(1, \boldsymbol{\xi}^\top\right)^\top \geq 0,\ \forall\, \boldsymbol{\xi} \in \mathbb{R}^{|\mathcal{M}|},\ \boldsymbol{\pi} \in \mathit{vert}\,(\mathcal{Y}), \tag{EC.16}$$

$$\Leftrightarrow \exists \boldsymbol{\lambda}_1, \boldsymbol{\lambda}_2 \geq \mathbf{0}, \mathbf{V} \succeq 0,\ \forall\, \boldsymbol{\pi} \in \mathit{vert}\,(\mathcal{Y}), \tag{EC.17}$$

where

$$\mathbf{V} = \begin{bmatrix} r - \psi_1(\mathbf{x}, \boldsymbol{\pi}) - \boldsymbol{\lambda}_1^\top \mathbf{b}^{\text{ub}} + \boldsymbol{\lambda}_2^\top \mathbf{b}^{\text{lb}} & \frac{1}{2}\left(\mathbf{q} + \mathbf{A}^\top(\boldsymbol{\lambda}_1 - \boldsymbol{\lambda}_2) - \psi_2(\boldsymbol{\pi})\right)^\top \\ \frac{1}{2}\left(\mathbf{q} + \mathbf{A}^\top(\boldsymbol{\lambda}_1 - \boldsymbol{\lambda}_2) - \psi_2(\boldsymbol{\pi})\right) & \mathbf{Q} \end{bmatrix}.$$

The first equivalence (EC.16) holds due to the definition of $\mathbf{V}$. For the second equivalence, $\Leftarrow$ follows from the definition of a positive semidefinite (PSD) matrix. To prove $\Rightarrow$, we consider an arbitrary vector $(\zeta_0 \in \mathbb{R}, \boldsymbol{\zeta}^\top \in \mathbb{R}^{|\mathcal{M}|})^\top \in \mathbb{R}^{|\mathcal{M}|+1}$: (1) if $\zeta_0 = 0$, then $(\zeta_0, \boldsymbol{\zeta}^\top)\mathbf{V}(\zeta_0, \boldsymbol{\zeta}^\top)^\top = \boldsymbol{\zeta}^\top \mathbf{Q} \boldsymbol{\zeta} \geq 0$ because $\mathbf{Q}$ is PSD; (2) if $\zeta_0 \neq 0$, then we have $(\zeta_0, \boldsymbol{\zeta}^\top)\mathbf{V}(\zeta_0, \boldsymbol{\zeta}^\top)^\top = \zeta_0^2 (1, \boldsymbol{\zeta}^\top/\zeta_0)\mathbf{V}(1, \boldsymbol{\zeta}^\top/\zeta_0)^\top \geq 0$, because of (EC.16). Therefore, $\Rightarrow$ holds.

We obtain Problem $(\mathcal{P}_{\text{F}})$ by replacing constraints (13) in Problem $(\mathcal{P}'_{\text{in}})$ with (EC.17) and further combine Problem $(\mathcal{P}'_{\text{in}})$ with the outer minimization problem in $(\mathcal{P}_{\text{M}})$.

□

Appendix D: Proof of Proposition 3

We can describe the inner maximization problem $\max_{\mathbb{P} \in \mathcal{D}} \mathbb{E}_{\mathbb{P}}[f(\mathbf{x}, \boldsymbol{\xi})]$ in Problem $(\mathcal{P}_{\text{M}})$ as

$$\max_{\mathbb{P} \in \mathcal{D}} \int_{\boldsymbol{\Omega}} f(\mathbf{x}, \boldsymbol{\xi})\, d\mathbb{P}(\boldsymbol{\xi}) \tag{EC.18}$$

$$\text{s.t.} \int_{\boldsymbol{\Omega}} d\mathbb{P}(\boldsymbol{\xi}) = 1, \tag{EC.19}$$

$$\int_{\boldsymbol{\Omega}} \begin{bmatrix} \boldsymbol{\Sigma} & \boldsymbol{\xi} - \boldsymbol{\mu} \\ (\boldsymbol{\xi} - \boldsymbol{\mu})^\top & \gamma_1 \end{bmatrix} d\mathbb{P}(\boldsymbol{\xi}) \succeq 0, \tag{EC.20}$$

$$\int_{\boldsymbol{\Omega}} (\boldsymbol{\xi} - \boldsymbol{\mu})(\boldsymbol{\xi} - \boldsymbol{\mu})^\top d\mathbb{P}(\boldsymbol{\xi}) \preceq \gamma_2 \boldsymbol{\Sigma}. \tag{EC.21}$$

Let r, $\begin{bmatrix} \mathbf{P} & \mathbf{p} \\ \mathbf{p}^\top & s \end{bmatrix} \succeq 0$, and $\mathbf{Q} \succeq 0$ be Lagrangian multipliers of constraints (EC.19), (EC.20), and (EC.21), respectively. With any given $\mathbf{x} \in \mathcal{X}$, where $\mathcal{X} = \{\mathbf{x} \mid (1) - (2)\}$, the Lagrangian dual problem of (EC.18) is

$$\begin{aligned} \min_{r, \mathbf{Q}, \mathbf{P}, \mathbf{p}, s}\ & r + \left(\gamma_2 \boldsymbol{\Sigma} - \boldsymbol{\mu}\boldsymbol{\mu}^\top\right) \bullet \mathbf{Q} + \boldsymbol{\Sigma} \bullet \mathbf{P} - 2\boldsymbol{\mu}^\top \mathbf{p} + \gamma_1 s \\ \text{s.t. }\ & \boldsymbol{\xi}^\top \mathbf{Q} \boldsymbol{\xi} - 2\boldsymbol{\xi}^\top (\mathbf{p} + \mathbf{Q}\boldsymbol{\mu}) + r - f(\mathbf{x}, \boldsymbol{\xi}) \geq 0,\ \forall\, \boldsymbol{\xi} \in \Omega, \\ & \mathbf{Q} \succeq 0, \\ & \begin{bmatrix} \mathbf{P} & \mathbf{p} \\ \mathbf{p}^\top & s \end{bmatrix} \succeq 0. \end{aligned} \tag{EC.22}$$

Our conditions on γ_1, γ_2, and $\boldsymbol{\Sigma}$ are sufficient to ensure that the Dirac measure $\delta_{\boldsymbol{\mu}}$ lies in the relative interior of the feasible set of $\max_{\mathbb{P} \in \mathcal{D}} \mathbb{E}_{\mathbb{P}}[f(\mathbf{x}, \boldsymbol{\xi})]$. Therefore, by the weaker version of Proposition 3.4 in Shapiro (2001), we can conclude that there is no duality gap between Problems (EC.18) and (EC.22). Consequently, Problem $(\mathcal{P}_{\text{M}})$ has the same optimal value as the following problem:

$$\min_{\substack{\mathbf{x} \in \mathcal{X} \\ r, \mathbf{Q}, \mathbf{P}, \mathbf{p}, s}} \mathbf{c}^\top \mathbf{x} + r + \left(\gamma_2 \boldsymbol{\Sigma} - \boldsymbol{\mu}\boldsymbol{\mu}^\top\right) \bullet \mathbf{Q} + \boldsymbol{\Sigma} \bullet \mathbf{P} - 2\boldsymbol{\mu}^\top \mathbf{p} + \gamma_1 s \tag{EC.23}$$

$$\begin{aligned}
&\text{s.t. } \boldsymbol{\xi}^\top \mathbf{Q}\boldsymbol{\xi} - 2\boldsymbol{\xi}^\top (\mathbf{p} + \mathbf{Q}\boldsymbol{\mu}) + r - f(\mathbf{x}, \boldsymbol{\xi}) \geq 0,\ \forall \boldsymbol{\xi} \in \Omega,\\
&\quad \mathbf{Q} \succeq 0,\\
&\quad \begin{bmatrix} \mathbf{P} & \mathbf{p} \\ \mathbf{p}^\top & s \end{bmatrix} \succeq 0.
\end{aligned}$$

We let $(\mathbf{x}^*, r^*, \mathbf{Q}^*, \mathbf{P}^*, \mathbf{p}^*, s^*)$ be the optimal solution of Problem (EC.23) when $\boldsymbol{\Sigma} = \boldsymbol{\Sigma}''$, and its optimal value equals $\Gamma(\boldsymbol{\Sigma}'')$. This solution is obviously feasible to Problem (EC.23) with any other values of $\boldsymbol{\Sigma}$. Therefore, for any $\boldsymbol{\Sigma}' \preceq \boldsymbol{\Sigma}''$, we have

$$\Gamma(\boldsymbol{\Sigma}') \leq \mathbf{c}^\top \mathbf{x}^* + r^* + \left(\gamma_2 \boldsymbol{\Sigma}' - \boldsymbol{\mu}\boldsymbol{\mu}^\top\right) \bullet \mathbf{Q}^* + \boldsymbol{\Sigma}' \bullet \mathbf{P}^* - 2\boldsymbol{\mu}^\top \mathbf{p}^* + \gamma_1 s^*.$$

This follows that

$$\begin{aligned}
\Gamma(\boldsymbol{\Sigma}'') - \Gamma(\boldsymbol{\Sigma}') &= \left(\mathbf{c}^\top \mathbf{x}^* + r^* + \left(\gamma_2 \boldsymbol{\Sigma}'' - \boldsymbol{\mu}\boldsymbol{\mu}^\top\right) \bullet \mathbf{Q}^* + \boldsymbol{\Sigma}'' \bullet \mathbf{P}^* - 2\boldsymbol{\mu}^\top \mathbf{p}^* + \gamma_1 s^*\right) - \Gamma(\boldsymbol{\Sigma}')\\
&\geq \left(\mathbf{c}^\top \mathbf{x}^* + r^* + \left(\gamma_2 \boldsymbol{\Sigma}'' - \boldsymbol{\mu}\boldsymbol{\mu}^\top\right) \bullet \mathbf{Q}^* + \boldsymbol{\Sigma}'' \bullet \mathbf{P}^* - 2\boldsymbol{\mu}^\top \mathbf{p}^* + \gamma_1 s^*\right)\\
&\quad - \left(\mathbf{c}^\top \mathbf{x}^* + r^* + \left(\gamma_2 \boldsymbol{\Sigma}' - \boldsymbol{\mu}\boldsymbol{\mu}^\top\right) \bullet \mathbf{Q}^* + \boldsymbol{\Sigma}' \bullet \mathbf{P}^* - 2\boldsymbol{\mu}^\top \mathbf{p}^* + \gamma_1 s^*\right)\\
&= \left(\boldsymbol{\Sigma}'' - \boldsymbol{\Sigma}'\right) \bullet \left(\gamma_2 \mathbf{Q}^* + \mathbf{P}^*\right).
\end{aligned}$$

Because $\begin{bmatrix} \mathbf{P}^* & \mathbf{p}^* \\ \mathbf{p}^{*\top} & s^* \end{bmatrix} \succeq 0$ and $\mathbf{P}^*$ is its principal submatrix, we have $\mathbf{P}^* \succeq 0$. Furthermore, because $\mathbf{Q}^* \succeq 0$ and $\gamma_2 \geq 0$, we then have $\gamma_2 \mathbf{Q}^* + \mathbf{P}^* \succeq 0$. Since $\boldsymbol{\Sigma}' \preceq \boldsymbol{\Sigma}''$, we also have $\boldsymbol{\Sigma}'' - \boldsymbol{\Sigma}' \succeq 0$. Therefore, we can have $(\boldsymbol{\Sigma}'' - \boldsymbol{\Sigma}') \bullet (\gamma_2 \mathbf{Q}^* + \mathbf{P}^*) \geq 0$, which immediately follows that $\Gamma(\boldsymbol{\Sigma}'') - \Gamma(\boldsymbol{\Sigma}') \geq 0$.

□

Appendix E: Proof of Proposition 4

Let $\mathbf{x}^*$ be the optimal solution of Problem (14). It is trivial that $\mathbf{x}^*$ is feasible to Problem $(\mathcal{P}_{\mathrm{M}})$ for any $\boldsymbol{\Sigma} \succeq 0$. Therefore, we have

$$\Gamma(\boldsymbol{\Sigma}) \leq \mathbf{c}^\top \mathbf{x}^* + \max_{\mathbb{P} \in \mathcal{D}} \mathbb{E}_{\mathbb{P}}\left[f(\mathbf{x}^*, \boldsymbol{\xi})\right] \leq \mathbf{c}^\top \mathbf{x}^* + \max_{\mathbb{P} \in \mathcal{D}_1} \mathbb{E}_{\mathbb{P}}\left[f(\mathbf{x}^*, \boldsymbol{\xi})\right] = \overline{\Gamma},$$

where the second inequality holds because $\mathcal{D} \subseteq \mathcal{D}_1$.

□

Appendix F: Proof of Proposition 5

Let $\epsilon > 0$ denote an arbitrary small number, and $\boldsymbol{\Sigma}^{\mathrm{d}}_{i,i} = \boldsymbol{\Sigma}_{i,i} - \sum_{j \in \{1,\ldots,|\mathcal{M}|\}, j \neq i} |\boldsymbol{\Sigma}_{i,j}| - \epsilon$ for any $i \in \{1, \ldots, |\mathcal{M}|\}$. Since $\sum_{j \in \{1,\ldots,|\mathcal{M}|\}, j \neq i} |\boldsymbol{\Sigma}_{i,j}| < \boldsymbol{\Sigma}_{i,i}$ for any $i \in \{1, \ldots, |\mathcal{M}|\}$, we have $\boldsymbol{\Sigma}^{\mathrm{d}} \succeq 0$. Moreover, for any $\mathbf{v} \in \mathbb{R}^{|\mathcal{M}|}$, we have

$$\begin{aligned}
\mathbf{v}^\top \left(\boldsymbol{\Sigma} - \boldsymbol{\Sigma}^{\mathrm{d}}\right) \mathbf{v} &= \sum_{i=1}^{|\mathcal{M}|} \left(\boldsymbol{\Sigma}_{i,i} - \boldsymbol{\Sigma}^{\mathrm{d}}_{i,i}\right) \mathbf{v}_i^2 + \sum_{i=1}^{|\mathcal{M}|} \sum_{j \in \{1,\ldots,|\mathcal{M}|\}, j \neq i} \left(\boldsymbol{\Sigma}_{i,j} - \boldsymbol{\Sigma}^{\mathrm{d}}_{i,j}\right) \mathbf{v}_i \mathbf{v}_j\\
&= \sum_{i=1}^{|\mathcal{M}|} \left(\sum_{j \in \{1,\ldots,|\mathcal{M}|\}, j \neq i} |\boldsymbol{\Sigma}_{i,j}| + \epsilon \right) \mathbf{v}_i^2 + \sum_{i=1}^{|\mathcal{M}|} \sum_{j \in \{1,\ldots,|\mathcal{M}|\}, j \neq i} \boldsymbol{\Sigma}_{i,j} \mathbf{v}_i \mathbf{v}_j\\
&\geq \sum_{i=1}^{|\mathcal{M}|} \sum_{j \in \{1,\ldots,|\mathcal{M}|\}, j \neq i} |\boldsymbol{\Sigma}_{i,j}| \mathbf{v}_i^2 + \sum_{i=1}^{|\mathcal{M}|} \sum_{j \in \{1,\ldots,|\mathcal{M}|\}, j \neq i} \boldsymbol{\Sigma}_{i,j} \mathbf{v}_i \mathbf{v}_j
\end{aligned}$$

$$
\begin{aligned}
&\geq \sum_{i=1}^{|\mathcal{M}|} \sum_{j\in\{1,\ldots,|\mathcal{M}|\},j\neq i} |\mathbf{\Sigma}_{i,j}|\mathbf{v}_i^2 - \sum_{i=1}^{|\mathcal{M}|} \sum_{j\in\{1,\ldots,|\mathcal{M}|\},j\neq i} \left|\mathbf{\Sigma}_{i,j}\mathbf{v}_i\mathbf{v}_j\right| \\
&= \sum_{i=1}^{|\mathcal{M}|} \sum_{j\in\{1,\ldots,|\mathcal{M}|\},j\neq i} \left(|\mathbf{\Sigma}_{i,j}|\mathbf{v}_i^2 - |\mathbf{\Sigma}_{i,j}||\mathbf{v}_i||\mathbf{v}_j|\right) \\
&= \sum_{i=1}^{|\mathcal{M}|} \sum_{j>i}^{|\mathcal{M}|} |\mathbf{\Sigma}_{i,j}| \left(|\mathbf{v}_i| - |\mathbf{v}_j|\right)^2 \\
&\geq 0.
\end{aligned}
$$

Consequently, we have $\mathbf{\Sigma} - \mathbf{\Sigma}^{\mathrm{d}} \succeq 0$. By Proposition 3, we have $\Gamma(\mathbf{\Sigma}^{\mathrm{d}}) \leq \Gamma(\mathbf{\Sigma})$.

□

Appendix G: Proof of Proposition 6

Recall that with any given allocation decision $\mathbf{x} \in \mathcal{X}$, the Lagrangian dual problem of the inner maximization problem $\max_{\mathbb{P}\in\mathcal{D}} \mathbb{E}_{\mathbb{P}}[f(\mathbf{x},\boldsymbol{\xi})]$ in Problem $(\mathcal{P}_{\mathrm{M}})$ is

$$
\begin{aligned}
\min_{r,\mathbf{Q},\mathbf{P},\mathbf{p},s}\ & r + \left(\gamma_2\mathbf{\Sigma} - \boldsymbol{\mu}\boldsymbol{\mu}^\top\right) \bullet \mathbf{Q} + \mathbf{\Sigma} \bullet \mathbf{P} - 2\boldsymbol{\mu}^\top\mathbf{p} + \gamma_1 s \\
\text{s.t. } & \boldsymbol{\xi}^\top\mathbf{Q}\boldsymbol{\xi} - 2\boldsymbol{\xi}^\top(\mathbf{p} + \mathbf{Q}\boldsymbol{\mu}) + r - f(\mathbf{x},\boldsymbol{\xi}) \geq 0,\ \forall \boldsymbol{\xi} \in \Omega, \qquad \text{(EC.24)} \\
& \mathbf{Q} \succeq 0, \\
& \begin{bmatrix} \mathbf{P} & \mathbf{p} \\ \mathbf{p}^\top & s \end{bmatrix} \succeq 0.
\end{aligned}
$$

We obtain (EC.24) from the term of the Lagrangian function of $\max_{\mathbb{P}\in\mathcal{D}} \mathbb{E}_{\mathbb{P}}[f(\mathbf{x},\boldsymbol{\xi})]$:

$$
\int_{\boldsymbol{\xi}\in\Omega} \left(\boldsymbol{\xi}^\top\mathbf{Q}\boldsymbol{\xi} - 2\boldsymbol{\xi}^\top(\mathbf{p} + \mathbf{Q}\boldsymbol{\mu}) + r - f(\mathbf{x},\boldsymbol{\xi})\right) d\mathbb{P}(\boldsymbol{\xi}). \qquad \text{(EC.25)}
$$

When optimality is achieved, the complementarity conditions of the infinite-dimensional optimization duality hold (Section 5 of Shapiro 2001), which suggests that the integrand in (EC.25) is 0 based on $\mathrm{supp}(\mathbb{P}^*)$, i.e., the support set associated with the optimal distribution. Therefore, we have

$$
\int_{\boldsymbol{\xi}\in\mathrm{supp}(\mathbb{P}^*)} \left(\boldsymbol{\xi}^\top\mathbf{Q}\boldsymbol{\xi} - 2\boldsymbol{\xi}^\top(\mathbf{p} + \mathbf{Q}\boldsymbol{\mu}) + r - f(\mathbf{x},\boldsymbol{\xi})\right) d\mathbb{P}(\boldsymbol{\xi}) = 0. \qquad \text{(EC.26)}
$$

By definition of support set, we have $d\mathbb{P}(\boldsymbol{\xi}) > 0$ for any $\boldsymbol{\xi} \in \mathrm{supp}(\mathbb{P}^*)$. These, together with (EC.24), indicate

$$
\mathcal{V}(\boldsymbol{\xi}) := \boldsymbol{\xi}^\top\mathbf{Q}\boldsymbol{\xi} - 2\boldsymbol{\xi}^\top(\mathbf{p} + \mathbf{Q}\boldsymbol{\mu}) + r - f(\mathbf{x},\boldsymbol{\xi}) = 0,\ \forall \boldsymbol{\xi} \in \mathrm{supp}(\mathbb{P}^*).
$$

Therefore, for $\boldsymbol{\xi} + \delta_i\mathbf{e}_i, \boldsymbol{\xi} + \delta_j\mathbf{e}_j, \boldsymbol{\xi} + \delta_i\mathbf{e}_i + \delta_j\mathbf{e}_j \in \mathrm{supp}(\mathbb{P}^*)$, we have

$$
\begin{aligned}
0 &= \left(\mathcal{V}(\boldsymbol{\xi} + \delta_i\mathbf{e}_i + \delta_j\mathbf{e}_j) - \mathcal{V}(\boldsymbol{\xi} + \delta_j\mathbf{e}_j)\right) - \left(\mathcal{V}(\boldsymbol{\xi} + \delta_i\mathbf{e}_i) - \mathcal{V}(\boldsymbol{\xi})\right) \\
&= \Big(f(\mathbf{x},\boldsymbol{\xi} + \delta_j\mathbf{e}_j) - f(\mathbf{x},\boldsymbol{\xi} + \delta_i\mathbf{e}_i + \delta_j\mathbf{e}_j) - 2\delta_i\mathbf{e}_i^\top(\mathbf{p}^* + \mathbf{Q}^*\boldsymbol{\mu}) + \delta_i^2\mathbf{e}_i^\top\mathbf{Q}^*\mathbf{e}_i + 2\delta_i\left(\boldsymbol{\xi} + \delta_j\mathbf{e}_j\right)^\top\mathbf{Q}^*\mathbf{e}_i\Big) \\
&\quad - \Big(f(\mathbf{x},\boldsymbol{\xi}) - f(\mathbf{x},\boldsymbol{\xi} + \delta_i\mathbf{e}_i) - 2\delta_i\mathbf{e}_i^\top(\mathbf{p}^* + \mathbf{Q}^*\boldsymbol{\mu}) + \delta_i^2\mathbf{e}_i^\top\mathbf{Q}^*\mathbf{e}_i + 2\delta_i\boldsymbol{\xi}^\top\mathbf{Q}^*\mathbf{e}_i\Big) \\
&= \left(f(\mathbf{x},\boldsymbol{\xi} + \delta_j\mathbf{e}_j) - f(\mathbf{x},\boldsymbol{\xi} + \delta_i\mathbf{e}_i + \delta_j\mathbf{e}_j)\right) - \left(f(\mathbf{x},\boldsymbol{\xi}) - f(\mathbf{x},\boldsymbol{\xi} + \delta_i\mathbf{e}_i)\right) + 2\delta_i\delta_j\mathbf{e}_j^\top\mathbf{Q}^*\mathbf{e}_i \\
&= \left(f(\mathbf{x},\boldsymbol{\xi} + \delta_j\mathbf{e}_j) - f(\mathbf{x},\boldsymbol{\xi} + \delta_i\mathbf{e}_i + \delta_j\mathbf{e}_j)\right) - \left(f(\mathbf{x},\boldsymbol{\xi}) - f(\mathbf{x},\boldsymbol{\xi} + \delta_i\mathbf{e}_i)\right) + 2\delta_i\delta_j\mathbf{Q}^*_{i,j},
\end{aligned}
$$

which immediately follows (15). □

Appendix H: Proof of Theorem 2

The proof of the reformulation (17) is the same as that of Theorem 1 and thus is omitted here. By Theorem 2 in Cheramin et al. (2022), we have

$$\max_{\mathbb{P}_m \in \mathcal{D}_m} \mathbb{E}_{\mathbb{P}_m}\left[f\left(\mathbf{x}, \mathbf{U}_{|\mathcal{M}|\times m}\mathbf{\Lambda}_m^{\frac{1}{2}}\boldsymbol{\xi}_m + \boldsymbol{\mu}\right)\right] \leq \max_{\mathbb{P}\in\mathcal{D}} \mathbb{E}_{\mathbb{P}}\left[f\left(\mathbf{x}, \boldsymbol{\xi}\right)\right],$$

for any $\mathbf{x}$. This follows that

$$\sum_{z\in\mathcal{Z}}\sum_{s\in\mathcal{S}} c_s x_{z,s} + \max_{\mathbb{P}_m \in \mathcal{D}_m} \mathbb{E}_{\mathbb{P}_m}\left[f\left(\mathbf{x}, \mathbf{U}_{|\mathcal{M}|\times m}\mathbf{\Lambda}_m^{\frac{1}{2}}\boldsymbol{\xi}_m + \boldsymbol{\mu}\right)\right] \leq \sum_{z\in\mathcal{Z}}\sum_{s\in\mathcal{S}} c_s x_{z,s} + \max_{\mathbb{P}\in\mathcal{D}} \mathbb{E}_{\mathbb{P}}\left[f\left(\mathbf{x}, \boldsymbol{\xi}\right)\right],$$

for any $\mathbf{x}$ satisfying constraints (1) – (2).

Therefore,

$$\begin{aligned}
&\min_{\mathbf{x}}\left\{\sum_{z\in\mathcal{Z}}\sum_{s\in\mathcal{S}} c_s x_{z,s} + \max_{\mathbb{P}_m \in \mathcal{D}_m} \mathbb{E}_{\mathbb{P}_m}\left[f\left(\mathbf{x}, \mathbf{U}_{|\mathcal{M}|\times m}\mathbf{\Lambda}_m^{\frac{1}{2}}\boldsymbol{\xi}_m + \boldsymbol{\mu}\right)\right] \,\middle|\, (1)-(2)\right\} \\
&\leq \min_{\mathbf{x}}\left\{\sum_{z\in\mathcal{Z}}\sum_{s\in\mathcal{S}} c_s x_{z,s} + \max_{\mathbb{P}\in\mathcal{D}} \mathbb{E}_{\mathbb{P}}\left[f\left(\mathbf{x}, \boldsymbol{\xi}\right)\right] \,\middle|\, (1)-(2)\right\}.
\end{aligned}$$

Therefore, the optimal value of Problem (16) (i.e., Problem (17)) provides a lower bound for the optimal value of Problem ($\mathcal{P}_{\mathrm{M}}$).

By Theorem 2 in Cheramin et al. (2022), we have $\mathcal{D}_m \subset \mathcal{D}_{m_2}$ for $m_1 < m_2$. This follows that

$$\max_{\mathbb{P}_{m_1} \in \mathcal{D}_{m_1}} \mathbb{E}_{\mathbb{P}_{m_1}}\left[f\left(\mathbf{x}, \mathbf{U}_{|\mathcal{M}|\times m_1}\mathbf{\Lambda}_{m_1}^{\frac{1}{2}}\boldsymbol{\xi}_{m_1} + \boldsymbol{\mu}\right)\right] \leq \max_{\mathbb{P}_{m_2} \in \mathcal{D}_{m_2}} \mathbb{E}_{\mathbb{P}_{m_2}}\left[f\left(\mathbf{x}, \mathbf{U}_{|\mathcal{M}|\times m_2}\mathbf{\Lambda}_{m_2}^{\frac{1}{2}}\boldsymbol{\xi}_{m_2} + \boldsymbol{\mu}\right)\right]$$

for any $\mathbf{x}$. Therefore, we have

$$\begin{aligned}
&\min_{\mathbf{x}}\left\{\sum_{z\in\mathcal{Z}}\sum_{s\in\mathcal{S}} c_s x_{z,s} + \max_{\mathbb{P}_{m_1} \in \mathcal{D}_{m_1}} \mathbb{E}_{\mathbb{P}_{m_1}}\left[f\left(\mathbf{x}, \mathbf{U}_{|\mathcal{M}|\times m_1}\mathbf{\Lambda}_{m_1}^{\frac{1}{2}}\boldsymbol{\xi}_{m_1} + \boldsymbol{\mu}\right)\right] \,\middle|\, (1)-(2)\right\} \\
&\leq \min_{\mathbf{x}}\left\{\sum_{z\in\mathcal{Z}}\sum_{s\in\mathcal{S}} c_s x_{z,s} + \max_{\mathbb{P}_{m_2} \in \mathcal{D}_{m_2}} \mathbb{E}_{\mathbb{P}_{m_2}}\left[f\left(\mathbf{x}, \mathbf{U}_{|\mathcal{M}|\times m_2}\mathbf{\Lambda}_{m_2}^{\frac{1}{2}}\boldsymbol{\xi}_{m_2} + \boldsymbol{\mu}\right)\right] \,\middle|\, (1)-(2)\right\}.
\end{aligned}$$

That is, the optimal value of Problem (17) is nondecreasing in m_1.

Finally, Problem (16) is equivalent to Problem ($\mathcal{P}_{\mathrm{I}}$) (i.e., Problem ($\mathcal{P}_{\mathrm{M}}$)) when $m = |\mathcal{M}|$. Then, Problems (17) and ($\mathcal{P}_{\mathrm{M}}$) have the same optimal value. □

Appendix I: Proof of Proposition 7

The proof is similar with that of Propositions 1 and 2 and thus is omitted here. □

Appendix J: Proof of Theorem 3

The proof of the reformulation (20) is the same as that of Theorem 1 and thus is omitted here. By Theorem 4 in Cheramin et al. (2022), we have $\mathcal{D}_{\mathrm{I}} \subset \mathcal{D}_{\mathrm{U}}$. Therefore, for any $\mathbf{x}$, we have

$$\max_{\mathbb{P}_{\mathrm{I}} \in \mathcal{D}_{\mathrm{I}}} \mathbb{E}_{\mathbb{P}_{\mathrm{I}}}\left[f\left(\mathbf{x}, \mathbf{U}\mathbf{\Lambda}^{\frac{1}{2}}\boldsymbol{\xi}_{\mathrm{I}} + \boldsymbol{\mu}\right)\right] \leq \max_{\mathbb{P}_{\mathrm{U}} \in \mathcal{D}_{\mathrm{U}}} \mathbb{E}_{\mathbb{P}_{\mathrm{U}}}\left[f\left(\mathbf{x}, \mathbf{U}\mathbf{\Lambda}^{\frac{1}{2}}\boldsymbol{\xi}_{\mathrm{I}} + \boldsymbol{\mu}\right)\right].$$

This follows that

$$\sum_{z\in\mathcal{Z}}\sum_{s\in\mathcal{S}} c_s x_{z,s} + \max_{\mathbb{P}_{\mathrm{I}} \in \mathcal{D}_{\mathrm{I}}} \mathbb{E}_{\mathbb{P}_{\mathrm{I}}}\left[f\left(\mathbf{x}, \mathbf{U}\mathbf{\Lambda}^{\frac{1}{2}}\boldsymbol{\xi}_{\mathrm{I}} + \boldsymbol{\mu}\right)\right] \leq \sum_{z\in\mathcal{Z}}\sum_{s\in\mathcal{S}} c_s x_{z,s} + \max_{\mathbb{P}_{\mathrm{U}} \in \mathcal{D}_{\mathrm{U}}} \mathbb{E}_{\mathbb{P}_{\mathrm{U}}}\left[f\left(\mathbf{x}, \mathbf{U}\mathbf{\Lambda}^{\frac{1}{2}}\boldsymbol{\xi}_{\mathrm{I}} + \boldsymbol{\mu}\right)\right],$$

for any $\mathbf{x}$ satisfying constraints (1) – (2). Therefore,

$$\min_{\mathbf{x}} \left\{ \sum_{z\in\mathcal{Z}} \sum_{s\in\mathcal{S}} c_s x_{z,s} + \max_{\mathbb{P}_{\mathrm{I}}\in\mathcal{D}_{\mathrm{I}}} \mathbb{E}_{\mathbb{P}_{\mathrm{I}}} \left[f\left(\mathbf{x}, \mathbf{U}\boldsymbol{\Lambda}^{\frac{1}{2}}\boldsymbol{\xi}_{\mathrm{I}} + \boldsymbol{\mu}\right)\right] \,\middle|\, (1)-(2) \right\}$$
$$\leq \min_{\mathbf{x}} \left\{ \sum_{z\in\mathcal{Z}} \sum_{s\in\mathcal{S}} c_s x_{z,s} + \max_{\mathbb{P}_{\mathrm{U}}\in\mathcal{D}_{\mathrm{U}}} \mathbb{E}_{\mathbb{P}_{\mathrm{U}}} \left[f\left(\mathbf{x}, \mathbf{U}\boldsymbol{\Lambda}^{\frac{1}{2}}\boldsymbol{\xi}_{\mathrm{I}} + \boldsymbol{\mu}\right)\right] \,\middle|\, (1)-(2) \right\}.$$

Therefore, the optimal value of Problem (19) (i.e., Problem (20)) provides an upper bound for the optimal value of Problem ($\mathcal{P}_{\mathrm{I}}$) (i.e., Problem ($\mathcal{P}_{\mathrm{M}}$)). □

Appendix K: Proof of Proposition 8

This result is deduced from Proposition 5 in Cheramin et al. (2022). □

Appendix L: Formulations of Problems in Algorithm 2

For any sub-network $\mathcal{G}_l$, $l \in \{1,\ldots,L\}$, we let $\mathcal{M}_l := \{(z,t,z') \in \mathcal{Z}\times\mathcal{T}_l\times\mathcal{Z} | (n_{z,t,s}, n_{z',t',s'}) \in \mathcal{A}_l^{\mathrm{R}}\}$ denote the set of indices of all trip demands in $\mathcal{G}_l$. Let $\boldsymbol{\xi}_l$ denote a vector of (demand) uncertainties in sub-network $\mathcal{G}_l$, and $\boldsymbol{\xi}_l$ follows a distribution $\mathbb{P}_l$, for $l \in \{1,\ldots,L\}$.

Consequently, we formulate Problem ($\mathcal{P}_1$) based on sub-network $\mathcal{G}_l$ as the following:

$$\min_{\mathbf{x}} \left\{ \sum_{z\in\mathcal{Z}} \sum_{s\in\mathcal{S}} c_s x_{z,s} + \mathbb{E}_{\mathbb{P}_l}\left[f_l\left(\mathbf{x}, \boldsymbol{\xi}_l\right)\right] \,\middle|\, (1)-(2) \right\},$$

where

$$\begin{aligned}
f_l\left(\mathbf{x}, \boldsymbol{\xi}_l\right) = \min_{\mathbf{w}(\boldsymbol{\xi}_l)} \; & \sum_{a\in\mathcal{A}_l} c_a w_a(\boldsymbol{\xi}_l) + c_{\mathrm{P}} \sum_{(z,t,z')\in\mathcal{M}_l} \left(d_{z,t,z'}(\boldsymbol{\xi}_l) - \sum_{a\in\hat{\mathcal{A}}_l^{\mathrm{R}}(z,t,z')} w_a(\boldsymbol{\xi}_l) \right) \\
\text{s.t.} \; & \sum_{a\in\mathcal{A}_{l+}(n_{z,t_0,s})} w_a(\boldsymbol{\xi}_l) = x_{z,s}, \; \forall z\in\mathcal{Z}, s\in\mathcal{S}, \\
& \sum_{a\in\mathcal{A}_{l+}(n_{z,t,s})} w_a(\boldsymbol{\xi}_l) = \sum_{a\in\mathcal{A}_{l-}(n_{z,t,s})} w_a(\boldsymbol{\xi}_l), \; \forall t\in\{t_0+1,\ldots,t'-1\}, z\in\mathcal{Z}, s\in\mathcal{S}, \\
& \sum_{z\in\mathcal{Z}}\sum_{s\in\mathcal{S}} \sum_{a\in\mathcal{A}_{l-}(n_{z,t',s})} w_a(\boldsymbol{\xi}_l) = \sum_{z\in\mathcal{Z}}\sum_{s\in\mathcal{S}} x_{z,s}, \\
& \sum_{a\in\hat{\mathcal{A}}_l^{\mathrm{R}}(z,t,z')} w_a(\boldsymbol{\xi}_l) \leq d_{z,t,z'}(\boldsymbol{\xi}_l), \; \forall (z,t,z')\in\mathcal{M}_l, \\
& \sum_{s\in\mathcal{S}} \sum_{a\in\cup_{k\in\mathcal{K}}\mathcal{A}_{l+}^k(n_{z,t,s})} w_a(\boldsymbol{\xi}_l) \leq \sum_{k\in\mathcal{K}} X_z^k, \; \forall z\in\mathcal{Z}, t\in\mathcal{T}_l, \\
& \sum_{s\in\mathcal{S}} \sum_{a\in\mathcal{A}_{l+}^{\mathrm{C}}(n_{z,t,s})\cup\mathcal{A}_{l+}^{\mathrm{E}}(n_{z,t,s})} w_a(\boldsymbol{\xi}_l) \leq X_z^{\mathrm{C}} + X_z^{\mathrm{E}}, \; \forall z\in\mathcal{Z}, t\in\mathcal{T}_l, \\
& \sum_{s\in\mathcal{S}} \sum_{a\in\mathcal{A}_{l+}^{\mathrm{E}}(n_{z,t,s})} w_a(\boldsymbol{\xi}_l) \leq X_z^{\mathrm{E}}, \; \forall z\in\mathcal{Z}, t\in\mathcal{T}_l, \\
& w_a \geq 0, \; \forall a\in\mathcal{A}_l,
\end{aligned}$$

where $t_0 = 0$ if $l = 1$ and $t_0 = \sum_{i=1}^{l-1} T_i + 1$ otherwise, and $t' = \sum_{i=1}^{l} T_i$. Let Ω_l, $\boldsymbol{\mu}_l$, and $\boldsymbol{\Sigma}_l$ denote the support set, mean vector, and covariance matrix of the vector of uncertainties $\boldsymbol{\xi}_l$, for $l \in \{1,\ldots,L\}$. We define the SDP problem below:

$$\min_{\mathbf{x}} \left\{ \sum_{z\in\mathcal{Z}} \sum_{s\in\mathcal{S}} c_s x_{z,s} + \max_{\mathbb{P}_l\in\mathcal{D}_l} \mathbb{E}_{\mathbb{P}_l}\left[f_l\left(\mathbf{x}, \boldsymbol{\xi}_l\right)\right] \,\middle|\, (1)-(2) \right\}, \qquad (\mathcal{P}_{\mathrm{M}}^l)$$

where

$$\mathcal{D}(\Omega_l, \boldsymbol{\mu}_l, \boldsymbol{\Sigma}_l, \gamma_1, \gamma_2) = \left\{ \mathbb{P}_l \middle| \begin{array}{l} \mathbb{P}_l\left(\boldsymbol{\xi}_l \in \Omega_l\right) = 1 \\ \left(\mathbb{E}_{\mathbb{P}_l}[\boldsymbol{\xi}_l] - \boldsymbol{\mu}_l\right)^\top \boldsymbol{\Sigma}_l^{-1} \left(\mathbb{E}_{\mathbb{P}_l}[\boldsymbol{\xi}_l] - \boldsymbol{\mu}_l\right) \leq \gamma_1 \\ \mathbb{E}_{\mathbb{P}_l}\left[\left(\boldsymbol{\xi}_l - \boldsymbol{\mu}_l\right)\left(\boldsymbol{\xi}_l - \boldsymbol{\mu}_l\right)^\top\right] \preceq \gamma_2 \boldsymbol{\Sigma}_l \end{array} \right\}.$$

We add a subscript $l \in \{1, \ldots, L\}$ to each notation for each sub-network $\mathcal{G}_l$. We can then adopt the same reformulation sequence in Section 4 to transform Problem $(\mathcal{P}_{\mathrm{M}}^l)$ into a solvable model $(\mathcal{P}_{\mathrm{F}}^l)$, for $l \in \{1, \ldots, L\}$.

$$\min_{\substack{\mathbf{x}, \boldsymbol{\pi}_l \in vert(\mathcal{Y}_l) \\ \mathbf{Q}_l \succeq 0, \mathbf{q}_l, r_l \\ \boldsymbol{\lambda}_{1,l}, \boldsymbol{\lambda}_{2,l} \geq \mathbf{0}}} \sum_{z \in \mathcal{Z}} \sum_{s \in \mathcal{S}} c_s x_{z,s} + r_l + \left(\gamma_2 \boldsymbol{\Sigma}_l + \boldsymbol{\mu}_l \boldsymbol{\mu}_l^\top\right) \bullet \mathbf{Q}_l + \boldsymbol{\mu}_l^\top \mathbf{q}_l + \sqrt{\gamma_1} \left\| \boldsymbol{\Sigma}_l^{\frac{1}{2}} \left(\mathbf{q}_l + 2\mathbf{Q}_l \boldsymbol{\mu}_l\right) \right\|_2 \tag{$\mathcal{P}_{\mathrm{F}}^l$}$$

$$\text{s.t. } (1) - (2),$$

$$\begin{bmatrix} r_l - \psi_{1,l}\left(\mathbf{x}, \boldsymbol{\pi}_l\right) - \boldsymbol{\lambda}_{1,l}^\top \mathbf{b}_l^{\mathrm{ub}} + \boldsymbol{\lambda}_{2,l}^\top \mathbf{b}_l^{\mathrm{lb}} & \frac{1}{2}\left(\mathbf{q}_l + \mathbf{A}_l^\top \left(\boldsymbol{\lambda}_{1,l} - \boldsymbol{\lambda}_{2,l}\right) - \psi_{2,l}\left(\boldsymbol{\pi}_l\right)\right)^\top \\ \frac{1}{2}\left(\mathbf{q}_l + \mathbf{A}_l^\top \left(\boldsymbol{\lambda}_{1,l} - \boldsymbol{\lambda}_{2,l}\right) - \psi_{2,l}\left(\boldsymbol{\pi}_l\right)\right) & \mathbf{Q}_l \end{bmatrix} \succeq 0.$$

Endnotes

1. We calculate daily trip demands in the following regions: (i) the Financial District in Lower Manhattan (office region), (ii) Greenwich Village, SoHo, and East Village in Lower Manhattan (residence region), and (iii) the neighborhood of the Empire State Building and Flatiron Building in Midtown Manhattan (commerce region).
2. We randomly select 100 samples from TLC (2024) and observe that the largest trip in one period among these samples is 3928. Consequently, we set the upper bound as 4000.
3. We assume the total number of parking spots without charging/discharging facilities equals the upper bound of the total number of allocated EVs, i.e., $\sum_{z \in \mathcal{Z}} X_z^{\mathrm{N}} = \overline{X} = 4000$. We then divide all these parking spots to each region equally, leading to $X_z^{\mathrm{N}} = 4000/5 = 800$ for any $z \in \mathcal{Z}$. NYC DOT (2021) state that 40% of urban parking spaces will be equipped with charging piles by 2030. Therefore, we set $X_z^{\mathrm{C}} = 0.4 X_z^{\mathrm{N}} = 320$ for any $z \in \mathcal{Z}$. We observe that the number of bi-directional charging facilities is smaller than the number of charging facilities. We thus assume $X_z^{\mathrm{E}} = 0.5 X_z^{\mathrm{C}} = 160$ for any $z \in \mathcal{Z}$.
4. The typical battery capacity for an EV is 40 kWh, which can support a driving range of 168 miles (E.ON 2024). According to NYC DOT (2024), the speed limit in NYC is 25 mph. Therefore, one EV is supposed to run $168/25 \approx 6.5$ hours after one full charge.
5. Due to the popularity and rapidly increasing trend of fast chargers, we consider fast charging in our experiments. We consider a common fast-charging rate of 120 kW, which can charge a total of 120 kW $\times$ 1/6 hours = 20 kWh in one period. This amount is equivalent to $20/40 \times 38 = 19$ SoC units. We consider a common discharging rate of 15 kW, which can discharge a total of 15 kW $\times$ 1/6 hours = 2.5 kWh in one period. This amount is equivalent to $2.5/40 \times 38 \approx 2$ SoC units.
6. The actual rental rate charged by Zipcar is \$14 per hour or \$2.3 per period (UC Riverside 2024). The unit relocation cost, idle cost, and degradation cost are estimated from Zhang et al. (2021).
7. The cost of allocating an EV with SoC $s \in \mathcal{S}$ to any service region $z \in \mathcal{Z}$ equals the EV purchasing cost spread over each day, i.e., 72, plus the cost of charging the EV to SoC s, i.e., $0.15s$. The expected lifetime of an EV is 500000 miles (E.ON 2024). Assuming EVs run 24 hours a day at a speed of 25 mph, each EV is estimated to run for approximately $500000/(25 \times 24) \approx 833$ days. With an average price of 61488 dollars per EV (The New York Times 2023), the cost spread over each day equals approximately $61488/833 \approx 72$ dollars. The electricity price at the beginning of the day is \$0.1/kW and the degradation cost is \$0.05/kW. So charging an EV to SoC s costs $0.15s$.